

UNCLASSIFIED

AD NUMBER

AD868237

LIMITATION CHANGES

TO:

Approved for public release; distribution is unlimited. Document partially illegible.

FROM:

Distribution authorized to U.S. Gov't. agencies only; Administrative/Operational Use; APR 1970. Other requests shall be referred to National Aeronautics and Space Administration, Langley Research Center, Hampton, VA 23365. Document partially illegible.

AUTHORITY

AEDEC/USAF ltr dtd 27 Mar 1972

THIS PAGE IS UNCLASSIFIED

AEDC-TR-70-49

**ARCHIVE COPY
DO NOT LOAN**

Copy 1



**DAMPING-IN-PITCH DERIVATIVES
OF 120- AND 140-DEG BLUNTED CONES
AT MACH NUMBERS FROM 0.6 THROUGH 3**

**B. L. Uselton, T. O. Shadow, and A. C. Mansfield
ARO, Inc.**

April 1970

Each transmittal of this document outside the agencies of the U. S. Government must have prior approval of NASA, Langley Research Center, Hampton, Virginia 23365.

This document has been approved for public release and sale; its distribution is unlimited.

per AF letter 27 Mar. 72, XON, W.O. Cole

**PROPULSION WIND TUNNEL FACILITY
ARNOLD ENGINEERING DEVELOPMENT CENTER
AIR FORCE SYSTEMS COMMAND
ARNOLD AIR FORCE STATION, TENNESSEE**

PROPERTY OF U. S. AIR FORCE
AEDC LIBRARY
F40600 - 69 - C - 0001

AEDC TECHNICAL LIBRARY



5 0720 00032 7827

NOTICES

When U. S. Government drawings specifications, or other data are used for any purpose other than a definitely related Government procurement operation, the Government thereby incurs no responsibility nor any obligation whatsoever, and the fact that the Government may have formulated, furnished, or in any way supplied the said drawings, specifications, or other data, is not to be regarded by implication or otherwise, or in any manner licensing the holder or any other person or corporation, or conveying any rights or permission to manufacture, use, or sell any patented invention that may in any way be related thereto.

Qualified users may obtain copies of this report from the Defense Documentation Center.

References to named commercial products in this report are not to be considered in any sense as an endorsement of the product by the United States Air Force or the Government.

DAMPING-IN-PITCH DERIVATIVES
OF 120- AND 140-DEG BLUNTED CONES
AT MACH NUMBERS FROM 0.6 THROUGH 3

B. L. Uselton, T. O. Shadow, and A. C. Mansfield
ARO, Inc.

This document has been approved for public release
and sale; its distribution is unlimited.

*per AF letter, XON, 27 Mar 72
W.D. Cole*

~~Each transmittal of this document outside the agencies of
the U. S. Government must have prior approval of NASA,
Langley Research Center, Hampton, Virginia 23365.~~

FOREWORD

The work reported herein was sponsored by the National Aeronautics and Space Administration (NASA), Langley Research Center, Hampton, Virginia, under Program Element 921E 5. The test program consisted of two phases with Phase I being conducted for NASA-Langley and Phase II conducted for the Martin-Marietta Corporation, Denver Division.

The test results presented were obtained by personnel of the von Kármán Gas Dynamics Facility, ARO, Inc. (a subsidiary of Sverdrup & Parcel and Associates, Inc.) contract operator of the Arnold Engineering Development Center (AEDC), Air Force Systems Command (AFSC), Arnold Air Force Station, Tennessee, under Contract F40600-69-C-0001. The tests were conducted under ARO Project No. PT1019 from September 3 to November 1, 1969. The manuscript was submitted for publication on January 19, 1970.

Information in this report is embargoed under the Department of State International Traffic in Arms Regulations. This report may be released to foreign governments by departments or agencies of the U. S. Government subject to approval of NASA, Langley Research Center, or higher authority. Private individuals or firms require a Department of State export license.

This technical report has been reviewed and is approved.

George F. Garey
Lt Colonel, USAF
AF Representative, PWT
Directorate of Test

Roy R. Croy, Jr.
Colonel, USAF
Director of Test

ABSTRACT

Wind tunnel tests were conducted to determine the damping-in-pitch derivatives ($C_{m\dot{q}} + C_{m\dot{\alpha}}$) of 120- and 140-deg blunted, conical models with and without base fairings. Measurements were made with a forced-oscillation dynamic balance as the model oscillated ± 1.8 deg at angles of attack ranging from -5.9 to 39.4 deg. Data were obtained at nominal Mach numbers of 0.6 to 3 and at free-stream Reynolds numbers, based on maximum model diameter, ranging from 0.37×10^6 to 1.62×10^6 . In general for all configurations the damping derivatives at $\alpha = 0$ were a strong nonlinear function of Mach number and showed the models to be dynamically unstable at Mach numbers from about 1.1 to 2.1 . However, as angle of attack increased, model stability increased and the derivatives were found to vary in a less nonlinear manner with Mach number. At $M_\infty = 1.9, 2.3,$ and 2.65 Reynolds number effects were investigated and it was noted that the damping-in-pitch derivatives were influenced strongly by Reynolds number. Addition of different base fairings produced no large changes in the damping derivatives.

Each transmittal of this document outside the agencies of the U. S. Government must have prior approval of NASA, Langley Research Center, Hampton, Virginia 23365.

CONTENTS

	<u>Page</u>
ABSTRACT	iii
NOMENCLATURE	vii
I. INTRODUCTION	1
II. APPARATUS	
2.1 NASA Models	2
2.2 Martin Models	2
2.3 Balance	3
2.4 Wind Tunnels	3
III. PROCEDURE	
3.1 Test Procedure	4
3.2 Precision of Measurements	4
IV. RESULTS AND DISCUSSION	
4.1 Effects of Angle of Attack	5
4.2 Effects of Reynolds Number	6
4.3 Effects of Center-of-Gravity Location	6
4.4 Effects of Mach Number	6
4.5 Effects of Base Fairings	7
V. CONCLUSIONS	7
REFERENCES	8

APPENDIXES

I. ILLUSTRATIONS

Figure

1. Photographs of NASA Models	13
2. Model Geometry (NASA)	14
3. Photographs of Martin Models	16
4. Photographs of Martin Base Fairings	17
5. Model Geometry (Martin)	18
6. Installation Photographs and Details	21
7. Damping-in-Pitch Derivatives as a Function of Angle of Attack, Config. 721M, $x_{cg}/\ell = 1.252$	24
8. Damping-in-Pitch Derivatives as a Function of Angle of Attack, Configs. 622M and 711M, $x_{cg}/\ell = 1.000$	27

<u>Figure</u>	<u>Page</u>
9. Damping-in-Pitch Derivatives as a Function of Angle of Attack, Configs. 711N and 711M	29
10. Damping-in-Pitch Derivatives as a Function of Reynolds Number, Config. 721M, $x_{cg}/\ell = 1.252$	31
11. Effects of Reynolds Number, Config. 721M, $x_{cg}/\ell = 1.252$	32
12. Damping-in-Pitch Derivatives as a Function of Center-of-Gravity Location, Config. 7B1M	33
13. Damping-in-Pitch Derivatives as a Function of Mach Number, Config. 721M, $x_{cg}/\ell = 1.252$	35
14. Damping-in-Pitch Derivatives as a Function of Mach Number, Config. 724M, $x_{cg}/\ell = 1.252$, $Re_d \approx 0.57 \times 10^6$ to 0.87×10^6	36
15. Damping-in-Pitch Derivatives as a Function of Mach Number, Config. 720M, $x_{cg}/\ell = 1.252$, $Re_d \approx 0.58 \times 10^6$ to 0.88×10^6	37
16. Damping-in-Pitch Derivatives as a Function of Mach Number, Config. 612M, $x_{cg}/\ell = 0.831$	38
17. Damping-in-Pitch Derivatives as a Function of Mach Number, Config. 622M, $x_{cg}/\ell = 1.000$	39
18. Damping-in-Pitch Derivatives as a Function of Mach Number, Config. 620M, $x_{cg}/\ell = 1.000$	40
19. Damping-in-Pitch Derivatives as a Function of Mach Number, Config. 711N, $x_{cg}/\ell = 1.066$	41
20. Damping-in-Pitch Derivatives as a Function of Mach Number, Config. 611N, $x_{cg}/\ell = 0.704$, $Re_d \approx 0.39 \times 10^6$ to 0.58×10^6	42
21. Effect of Base Fairing, Config. 721M and 720M, $x_{cg}/\ell = 1.252$	43
22. Effect of Base Fairing, Config. 622M and 620M, $x_{cg}/\ell = 1.000$	46
23. Effect of Base Fairing, Config. 731M and 735M, $x_{cg}/\ell = 1.428$	48
24. Effect of Base Fairing, Config. 723M and 724M, $x_{cg}/\ell = 1.252$	50

	<u>Page</u>
II. TABLES	
I. Model Conditions	52
II. Tunnel Conditions	55

NOMENCLATURE.

A	Reference area (based on maximum model diameter), ft ²
C _D	Drag coefficient, drag/q _∞ A
C _m	Pitching-moment coefficient, pitching moment/q _∞ Ad
C _{m_q}	$\left. \begin{array}{l} \partial C_m / \partial (qd/2V_\infty) \\ \partial C_m / \partial (\dot{\alpha}d/2V_\infty) \end{array} \right\}$ Local damping-in-pitch deriva- tives, 1/radian
C _{m_{α̇}}	
C _{m_α}	Local slope of pitching-moment curve, 1/radian
d	Reference length (maximum model diameter), ft or in.
ℓ	Horizontal distance from model nose to maximum model diameter (see Fig. 2a), in.
M _∞	Free-stream Mach number
p ₀	Tunnel stilling chamber pressure, psia or psfa
q	Pitching velocity, radians/sec
q _∞	Free-stream dynamic pressure, lb/ft ² or psia
Re _d	Free-stream Reynolds number based on maximum model diameter
r _b	Maximum model radius, in.
r _n	Model nose radius, in.
T ₀	Tunnel stilling chamber temperature, °R
V _∞	Free-stream velocity, ft/sec
W	Vehicle weight, lb
x _{cg}	Distance from model nose to center of gravity (pivot axis) (see Fig. 2), in.

α	Angle of attack, radians or deg
$\dot{\alpha}$	Time rate of change of angle of attack, radians/sec
θ	Oscillation amplitude, deg
θ_{B1}, θ_{B2}	Base fairing angles (see Fig. 5c), deg
θ_c	Model cone half-angle (see Fig. 2a), deg
θ_m	Mean oscillation amplitude, deg
ω	Angular frequency, radians/sec
$\omega d/2V_\infty$	Reduced frequency parameter, radians

SUBSCRIPT

t Trim conditions

Note: Model configuration nomenclature is explained in Figs. 2 and 5.

SECTION I INTRODUCTION

The majority of the reentry research and development effort in the last decade has been directed toward reentry configurations for the earth atmosphere. Increased effort is now being directed toward the development of a planetary probe system capable of entering the atmosphere of Mars and landing a scientific payload. Although much of the extensive research and development effort expended upon the reentry vehicles for the earth atmosphere can be applied to the planetary exploration, major differences do exist. Primarily these differences are the result of very different atmospheric characteristics (low density relative to that of the earth) and higher entry velocities.

The requirements for a planetary probe system entering a Mars-type atmosphere have been evaluated, and the results indicate that a very low ballistic coefficient ($W/C_D A$) of the order of 3.2 to 6.4 lb/ft² will be required (Ref. 1). Additional requirements are that the configuration have high aerodynamic drag, inherent aerodynamic stability, sufficient volume to enclose the payload, and a relatively lightweight structure. Preliminary studies also showed that a configuration with high aerodynamic drag characteristics can use aerodynamic deceleration before actuation of terminal deceleration devices such as parachutes or retrorockets with an appreciable saving in system weight. Large-angle blunted cones, spherical segments, and tension shells are three shapes that have been considered for entering planetary atmospheres. Research and development groups are currently engaged in evaluating the aerodynamic characteristics of the candidate shapes in air and then determining the effects of Mars-type atmospheres on these aerodynamic characteristics. Several experimental tests have been conducted on planetary shapes to determine the static and dynamic aerodynamic characteristics for subsonic to hypersonic speeds (Refs. 1 through 14).

The Viking project is the NASA program for the exploration of the planet Mars using automated spacecraft. NASA-Langley has been assigned Viking project management and also detailed responsibility for the overall spacecraft and the lander. The Martin-Marietta Corporation, Denver Division, will provide the lander and assist NASA-Langley in integrating the lander with the orbiter and the resulting spacecraft with the launch vehicle.

In support of aerodynamic design programs conducted by NASA-Langley and Martin-Marietta Corporation on the blunt cone aeroshell, dynamic stability tests to investigate the effects of Mach number, Reynolds number, angle of attack, base geometry, and center-of-gravity location were conducted from subsonic to supersonic speeds. Phase I of the test program was conducted for NASA using models previously built for testing in the von Kármán Gas Dynamics Facility (VKF)(Ref. 14) and was in support of the Phase II test for Martin.

The present NASA and Martin tests were conducted on 120- and 140-deg blunted cones at Mach numbers from 0.6 through 3 at Reynolds numbers, based on maximum model diameter, of 0.37×10^6 to 1.62×10^6 . Data were obtained at oscillation amplitudes of ± 1.8 deg for an angle-of-attack range from -5.9 to 39.4 deg. The tests were conducted in the Propulsion Wind Tunnels (16T) and (16S) 16-ft transonic and supersonic wind tunnels using a small amplitude (± 3 deg) forced-oscillation balance.

SECTION II APPARATUS

2.1 NASA MODELS

The 10-in.-diam models (Fig. 1, Appendix I) were supplied by NASA-Langley and consisted of two stainless steel blunted cones having semivertex angles of 60 and 70 deg. These models were tested previously at supersonic Mach numbers in VKF (see Ref. 14). The bluntness ratio of the 120-deg model reported on in Ref. 14 is in error and should be the same as for the present tests ($r_n/r_b = 0.29$). For the present tests the bluntness ratio (r_n/r_b) of the 140-deg model was changed to 0.5, and both models were equipped with balsa wood afterbodies. Spacers were provided so that two pivot-axis locations could be tested, and weight rings were used to locate the center of gravity of the model at the pivot axis. Model geometries and specific model configuration designations are shown in Fig. 2.

2.2 MARTIN MODELS

The 15.5-in.-diam models (Fig. 3) were supplied by Martin-Marietta and consisted of two aluminum blunted forebody cones having semivertex angles of 60 and 70 deg and a bluntness ratio (r_n/r_b) of 0.5. Several different base fairing configurations (Fig. 4) were tested

on the forebody cones, and the forebody cones were also tested with only a balance shield (Fig. 3, Configs. 7B0M and 6B0M) attached to the base. Spacers were provided so that up to three center-of-gravity locations, depending on the configuration, could be tested. Provisions were made to add ballast fore and aft to locate the model center of gravity at the balance pivot axis. Model geometries and specific model configuration designations are shown in Fig. 5. The 140-deg forebody with base fairing 1 was the basic configuration and was used during the majority of the tests.

2.3 BALANCE

The small amplitude (± 3 deg), forced-oscillation balance system (Ref. 15) is a one-degree-of-freedom oscillatory system incorporating a cross-flexure pivot. During these tests, model oscillation amplitudes were approximately ± 1.8 deg. The balance is forced to oscillate by an electromagnetic shaker motor located in the aft portion of the sting. The angular displacement of the model is measured by a strain-gage bridge mounted on a cross flexure, and the input torque to the system is measured by a strain-gage bridge mounted at the minimum cross-sectional area of the torque beam. Whenever the model balance system was oscillated at a frequency other than its undamped natural frequency, electronic resolvers were used to determine the in-phase and out-of-phase components of the forcing torque signal. The forcing system is equipped with a feedback control network as described in Ref. 15 to provide positive amplitude control for testing either dynamically stable or unstable configurations.

2.4 WIND TUNNELS

Tunnel 16T is a variable density wind tunnel capable of operation from Mach numbers 0.20 to 1.60. The test section is 16 ft square by 40 ft long and is lined with perforated plates to allow continuous operation with minimum wall interference. The tunnel can be operated within a stagnation pressure (p_0) range from 80 to 4000 psfa depending on the Mach number.

Tunnel 16S is a variable density wind tunnel capable of operation between Mach numbers 1.5 and 4.75. Stagnation pressure can be varied from 180 to 2300 psfa depending on the Mach number.

Photographs and sketches of the test sections showing the location of the model and the support strut arrangements are shown in Fig. 6. A more extensive description of the tunnels is given in Ref. 16.

SECTION III PROCEDURE

3.1 TEST PROCEDURE

The model was oscillated at oscillation amplitudes of approximately ± 1.8 deg and the resulting time-resolved torque signal, in-phase and out-of-phase components of the torque signal, and displacement signal were recorded on magnetic tape by a high-speed digital converter and relayed to the computer for data reduction. The method used for reducing the data may be found in Ref. 17. A summary of the combinations of model configurations and wind tunnel test conditions is presented in Tables I and II, Appendix II.

3.2 PRECISION OF MEASUREMENTS

The balance was calibrated before and after the tests, and check calibrations were made before and after each run. In addition, structural damping values were obtained at vacuum conditions before the tunnel entry to evaluate the still-air damping contribution.

The precision of measurement of the damping derivative for previous tests at supersonic and hypersonic speeds using the forced-oscillation balance has normally been estimated to be about ± 6 percent or ± 0.02 in $C_{m\dot{q}} + C_{m\dot{\alpha}}$ for these tests. The spread in the present data is shown in the next section to be larger than this, particularly at the lower angles of attack ($\alpha < 3$ deg) and at the subsonic Mach numbers. This increased data spread can be partly attributed to installation vibration associated with the subsonic and transonic speed regime. Guy rods (see Fig. 6) were alternately used with various models to change the stiffness of the model sting support system so that the fundamental frequency of the support system was as far as possible from the model oscillation frequency. The aerodynamic phenomenon which caused the measured model instability at $\alpha = 0$ probably also contributed to the data spread. It will be of interest to note that as angle of attack increased and also as Mach number increased the data spread became less. Considering the above comments, it is estimated that the uncertainty in the data is about the same as the spread of the data.

The static stability parameter (local slope of the pitching-moment curve) is proportional to the difference of the square of the wind-on frequency and the square of the wind-off frequency. Since this frequency

change was less than 3 percent for the majority of the data, the estimated precision in the static stability parameter was quite large. For this reason, the static stability parameter data are not presented.

SECTION IV RESULTS AND DISCUSSION

4.1 EFFECTS OF ANGLE OF ATTACK

Typical angle-of-attack variations of the local values of the dynamic stability derivatives ($C_{m\dot{q}} + C_{m\dot{\alpha}}$) for Mach numbers from 0.6 to 3 for the NASA and Martin models are presented in Figs. 7 through 9. In general, these data show that for angles of attack of about 4 deg and above (for the angle-of-attack range that was investigated), the damping-in-pitch derivatives were essentially constant with angle of attack. At Mach numbers from 1 through 1.9 (for the Martin models, Figs. 7 and 8), at the low angles of attack ($0 \leq \alpha \lesssim 4$), the damping derivatives decreased sharply and became positive (negative damping) at $\alpha = 0$. The low angle-of-attack data at $M_\infty = 2.65$ (Fig. 7k) and $M_\infty = 3$ (Figs. 7l and 8g) show the damping derivatives started to decrease with angle of attack but at $\alpha = 0$ the configurations are dynamically stable. The data levels and trends are subject to change with Reynolds number and will be discussed in the following section. Because of the very small damping encountered at $\alpha = 0$ for the majority of the test conditions at Mach numbers from 0.6 to 0.9, the damping derivatives could not be measured.

Figure 8 also shows the effect of forebody cone angle on the damping derivatives for Mach numbers from 0.8 to 3. Both of these configurations had similar base fairings, and the center-of-gravity location was at the major diameter ($x_{CG}/l = 1$) for both configurations. There was no significant difference in the damping derivatives of 120- and 140-deg models except at $M_\infty = 1.9$ ($\alpha = 0$) where the 120-deg configuration (622M) is more unstable than the 140-deg configuration (711M).

Typical data from Phase I of the test program (NASA models) are shown in Fig. 9 for Mach numbers from 0.6 to 1.50. In general, data for the NASA models show about the same trends and levels as the data obtained on the Martin models except at $\alpha = 0$ where the NASA data generally show a larger level of instability than the Martin data.

4.2 EFFECTS OF REYNOLDS NUMBER

A limited Reynolds number investigation on the basic 140-deg configuration was conducted at Mach numbers 1.9, 2.3, and 2.65 (Fig. 10). The damping-in-pitch derivatives at $\alpha = 0$ showing both model stability and instability, were a strong function of Reynolds number and showed different trends at each Mach number. However, at $\alpha \approx 5.8$ deg, the model was stable for each Mach number and the derivatives decreased slightly as Reynolds number increased.

Model damping as a function of angle of attack for each Reynolds number at $M_\infty = 1.9, 2.3,$ and 2.65 is shown in Fig. 11a. The derivatives, depending on Mach number and Reynolds number, showed different trends with angle of attack. The angle-of-attack trends at $M_\infty = 2.3$ and 2.65 at Reynolds numbers where model dynamic stability exists throughout the angle-of-attack range tested show trends similar to those found at higher Mach numbers (see Fig. 7l and Ref. 14).

Figure 11b shows the effect of Reynolds number on the damping trends as a function of Mach number. Although there are not sufficient data to be conclusive, it appears that the damping trends are similar for the three Reynolds numbers tested. It is also of interest to note that the level of the damping derivatives at the lower Reynolds number ($Re_d \approx 0.4 \times 10^6$) at $M_\infty = 1.9$ approached more closely the level of the data obtained on the NASA models at the lower Mach numbers (Fig. 9) at $\alpha = 0$.

4.3 EFFECTS OF CENTER-OF-GRAVITY LOCATION

The effects of center-of-gravity location on the damping derivatives at Mach numbers from 0.7 to 3 for the basic 140-deg configuration (7B1M) are shown in Fig. 12. As model center of gravity was moved aft for $M_\infty = 1.1$ to 1.9 at $\alpha = 0$, model instability increased. At $M_\infty = 3$ ($\alpha = 0$) and for angles of attack of 2.9 deg and greater at all Mach numbers, center-of-gravity movement ($x_{cg}/l = 1$ to $x_{cg}/l = 1.428$) did not significantly affect the damping derivatives.

4.4 EFFECTS OF MACH NUMBER

The effects of Mach number on the dynamic stability derivatives at $\alpha = 0, 2.9,$ and 5.8 deg for several configurations are shown in Figs. 13 through 20. The damping derivatives at $\alpha = 0$ for $M_\infty = 1$ to 3 are a highly nonlinear function of Mach number for all configurations tested.

In general for a Mach number range of about 1.1 to approximately 2.1, the damping derivatives at $\alpha = 0$ for all configurations showed the models to be dynamically unstable. However, this is also a function of Reynolds number as has been discussed previously. At an angle of attack of 5.8 deg, the models were stable at all Mach numbers tested and the damping derivatives generally increased slightly with increasing Mach number.

4.5 EFFECTS OF BASE FAIRINGS

Comparisons of the data for the different base fairings are shown in Figs. 21 through 24. Figures 21 and 22 show the comparison of the damping derivatives as a function of angle of attack at $M_\infty = 0.7$ to 3 for the 140-deg (Fig. 21) and 120-deg (Fig. 22) configurations with and without the basic base fairing. In general the addition of the base fairing decreased the model damping; however, these differences are small and contained within the scatter of the data, except at $M_\infty = 3$ ($\alpha = 0$) where the addition of the fairing for both the 140- and 120- deg configurations (Figs. 21j and 22g, respectively) showed a definite decrease in model damping.

Figures 23 and 24 show the comparison of the damping derivatives of base fairings $C = 1$ with $C = 5$, and $C = 3$ with $C = 4$ on the 140-deg forebody at Mach numbers ranging from 0.7 to 1.4. The differences in the base fairing geometries for these comparisons produced no large effects on the damping derivatives.

SECTION V CONCLUSIONS

Wind tunnel tests were conducted to determine the effects of angle of attack, Mach number, Reynolds number, center-of-gravity location, and base fairing geometry on the damping-in-pitch derivatives of 120- and 140-deg blunted conical models with and without base fairings. Data were obtained over a Mach number range from 0.6 to 3 at free-stream Reynolds numbers, based on maximum model diameter, ranging from 0.37×10^6 to 1.62×10^6 . Conclusions based on the results presented in this report are given below:

1. All configurations were dynamically stable at angles of attack above approximately 4 deg for all Mach numbers and Reynolds numbers investigated.

2. The basic 140-deg configuration (721M)($x_{cg}/l = 1.252$) at $M_\infty = 1.9, 2.3,$ and 2.65 showed the levels and trends of the damping derivatives as a function of angle of attack for $0 \leq \alpha \lesssim 4$ deg to be strongly dependent on Reynolds number.
3. For all configurations the damping derivatives at $\alpha = 0$ were a highly nonlinear function of Mach number. For Mach numbers from about 1.1 to 2.1 at the Reynolds numbers tested, the data at $\alpha = 0$ showed all configurations to be unstable.
4. For an angle of attack of $\gtrsim 5.8$ deg, the damping derivatives for all configurations showed fairly smooth trends (slightly increasing) with Mach number.
5. At $M_\infty = 1.1, 1.2, 1.4, 1.6,$ and 1.9 for the basic 140-deg model, moving the center of gravity rearward at $\alpha = 0$ increased model instability. At $M_\infty = 3$ moving the center of gravity rearward produced no significant effect on model damping. In general, as angle of attack increased, the damping derivatives for the 140-deg basic configuration at all Mach numbers were affected less by movement of model center of gravity.
6. At all Mach numbers, addition of different base fairings to the 140-deg forebody produced no large changes in the trends or levels of the damping derivatives.

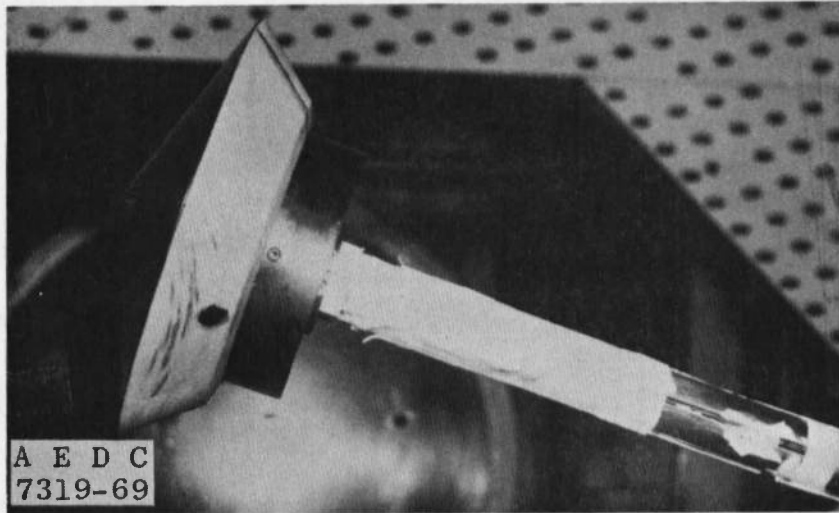
REFERENCES

1. Krumins, Maigonis V. "A Ballistic Range Study of Aerodynamic Characteristics of Mars Probe/Lander Shapes." AIAA Preprint No. 67-167, Fifth Aerospace Sciences Meeting, January 1967.
2. Marko, W. "Dynamic Stability of High-Drag Planetary Entry Vehicles at Transonic Speeds." AIAA Preprint No. 69-105, Seventh Aerospace Sciences Meeting, January 1969.
3. Bendura, Richard J. "Low Subsonic Static and Dynamic Stability Characteristics of Two Blunt 120° Cone Configurations." NASA-TN-D-3853, February 1967.
4. Campbell, James F. "Longitudinal Aerodynamic Characteristics of Several High-Drag Bodies at Mach Numbers from 1.5 to 4.63." NASA-TN-D-3915, April 1967.

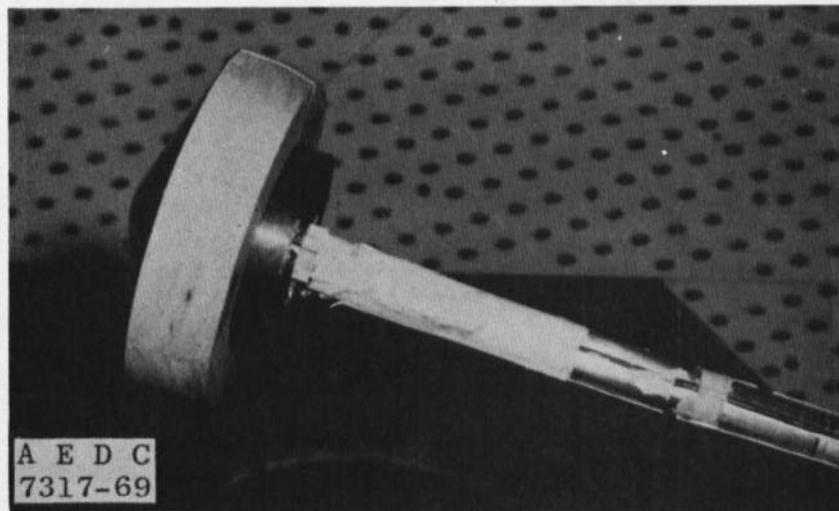
5. Campbell, James F. and Howell, Dorothy T. "Supersonic Aerodynamics of Large-Angle Cones." NASA-TN-D-4719, August 1968.
6. Walker, Billy and Weaver, Robert W. "Static Aerodynamic Characteristics of Blunted Cones in the Mach Number Range from 2.2 to 9.5." JPL-TR-32-1213, December 1967.
7. Marko, Wayne J. "Static Aerodynamic Characteristics of Three Blunted Sixty-Degree Half-Angle Cones at Mach Numbers from 0.60 to 1.30." JPL-TR-32-1298, July 1968.
8. Darnell, Wayne L., Henning, Allen B., and Lundstrom, Reginald R. "Flight Test of a 15-Ft-Diameter (4.6-Meter) 120° Conical Spacecraft Simulating Parachute Deployment in a Mars Atmosphere." NASA-TN-D-4266, December 1967.
9. Passamaneck, R. "Aerodynamic Characteristics of Spherically Blunted 45-Deg Half-Angle Cones." JPL-TR-32-1327, September 1968.
10. Whitlock, Charles H., Bendura, Richard J., and Henning, Allen B. "Dynamic Stability Characteristics of Large-Size 120° Blunted Conical Spacecraft in a Simulated Martian Environment." AIAA Preprint No. 69-104, Seventh Aerospace Sciences Meeting, January 1969.
11. Campbell, James F. and Grow, Josephine W. "Experimental Flow Properties in the Wake of a 120° Cone at Mach Number 2.20." NASA-TN-D-5365, July 1969.
12. Campbell, James F. "Supersonic Aerodynamic Characteristics and Shock Standoff Distances for Large-Angle Cones with and without Cylindrical Afterbodies." NASA-TN-D-5334, August 1969.
13. Deveikis, William D. and Sawyer, James Wayne. "Effects of Cone Angle, Base Flare Angle, and Corner Radius on Mach 3.0 Aerodynamic Characteristics of Large Angle Cones." NASA-TN-D-5048, March 1969.
14. Uselton, B. L. "Damping-in-Pitch Derivatives for 60- and 70-Deg Blunted Cones at Mach Numbers 3 through 5." AEDC-TR-69-119 (AD854436L), June 1969.
15. Welsh, C. J., Hance, Q. P., and Ward, L. K. "A Forced-Oscillation Balance System for the von Kármán Gas Dynamics Facility 40- by 40-Inch Supersonic Tunnel." AEDC-TN-61-63 (AD257380), May 1961.

16. Test Facilities Handbook (Eighth Edition). "Von Kármán Gas Dynamics Facility, Vol. 4." Arnold Engineering Development Center, December 1969.
17. Schueler, C. J., Ward, L. K., and Hodapp, A. E., Jr. "Techniques for Measurement of Dynamic Stability Derivatives in Ground Test Facilities." AGARDograph 121, October 1967.

APPENDIXES
I. ILLUSTRATIONS
II. TABLES

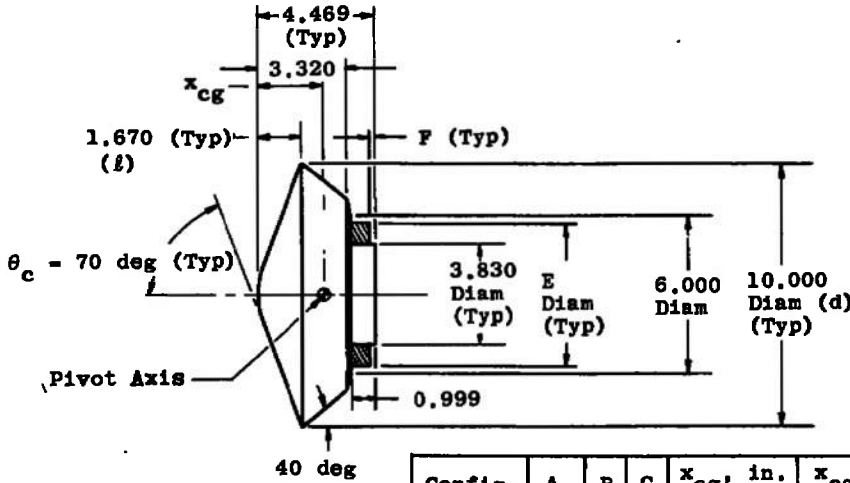


a. $\theta_c = 70$ deg, Config. 7B1N



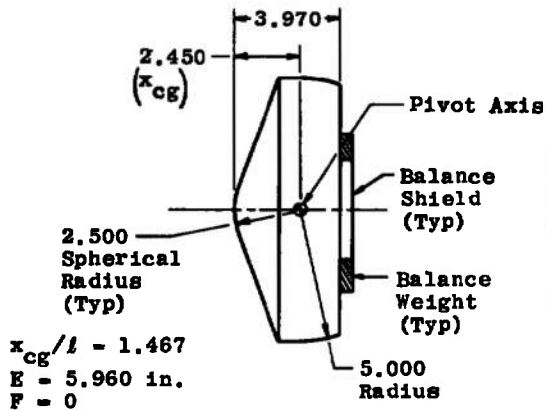
b. $\theta_c = 70$ deg, Config. 742N

Fig. 1 Photographs of NASA Models



Config.	A	B	C	x_{cg} , in.	x_{cg}/l	E, in.	F, in.
711N	70	1	1	1.780	1.066	4.330	0.428
741N	70	4	1	2.450	1.467	5.960	0

a. Config. 7B1N



Typical Model Nomenclature
Config. ABCD

where:

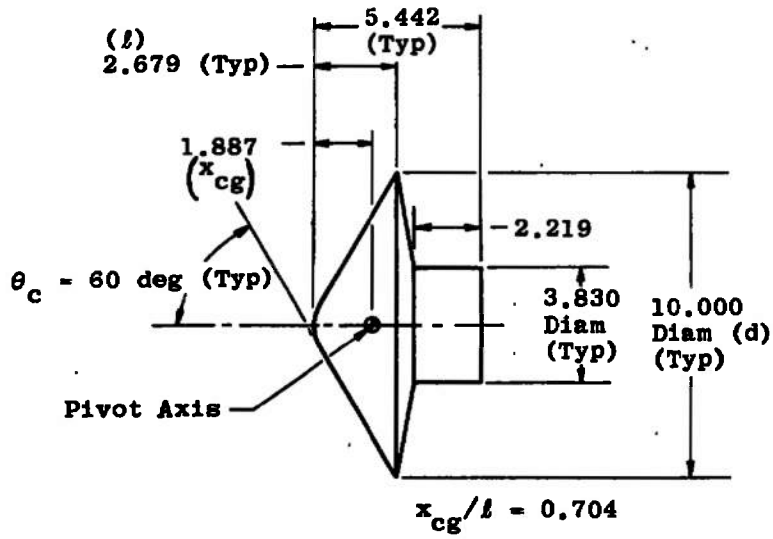
- A Cone Half-Angle, deg x 10⁻¹
- B Model Pivot Axis Location
- C Model Base Fairing
- D Cone Major Diameter

where:

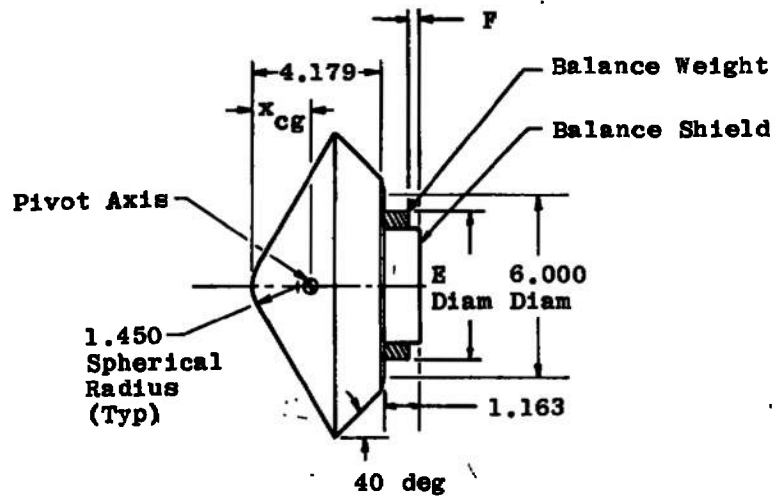
- C = 0 Denotes No Base Fairing
- C = 1 to 5 Denotes Base Fairing Used
- D = N Denotes d = 10 in. (NASA)
- D = M Denotes d = 15.5 in. (Martin)

All Dimensions in Inches

b. Config. 742N
Fig. 2 Model Geometry (NASA)



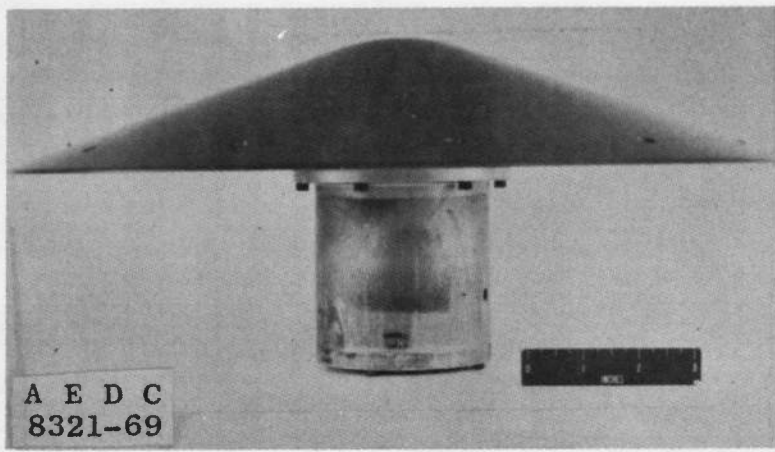
c. Config. 610N



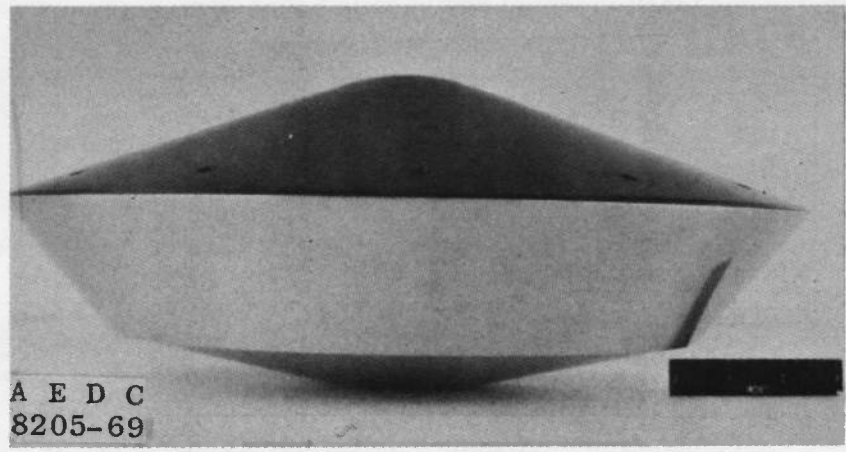
Config.	A	B	C	x_{cg} , in.	x_{cg}/l	E, in.	F, in.
611N	60	1	1	1.887	0.704	0	0
631N	60	3	1	2.679	1.000	4.830	0.334

All Dimensions in Inches

d. Config. 6B1N
Fig. 2 Concluded

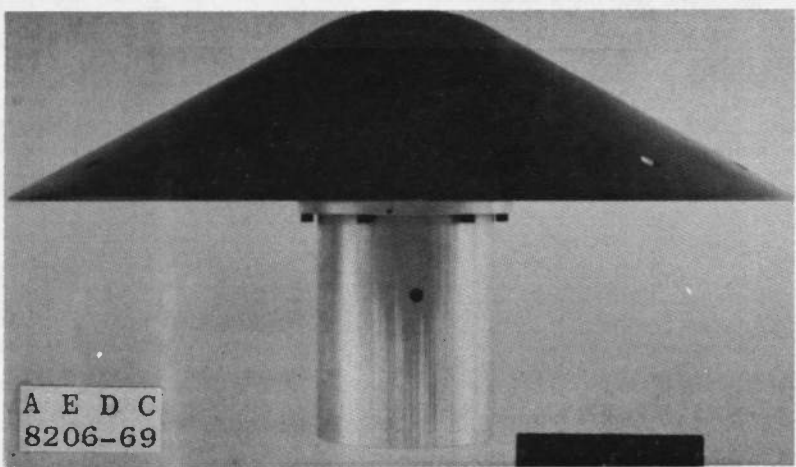


Config. 7B0M

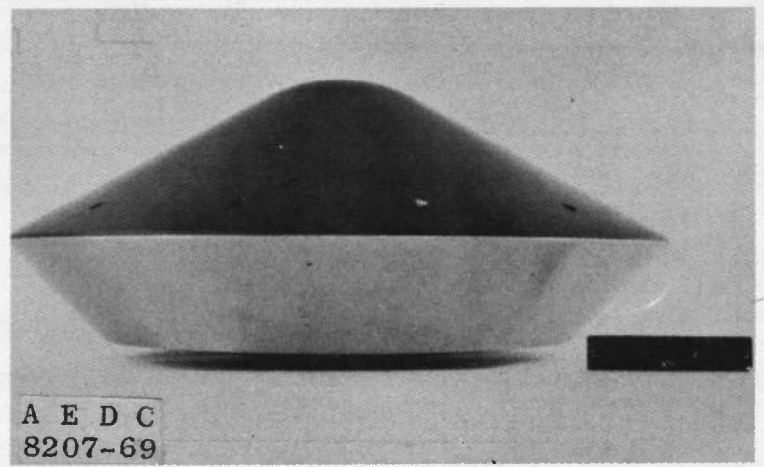


Config. 7B1M

a. $\theta_c = 70$ deg



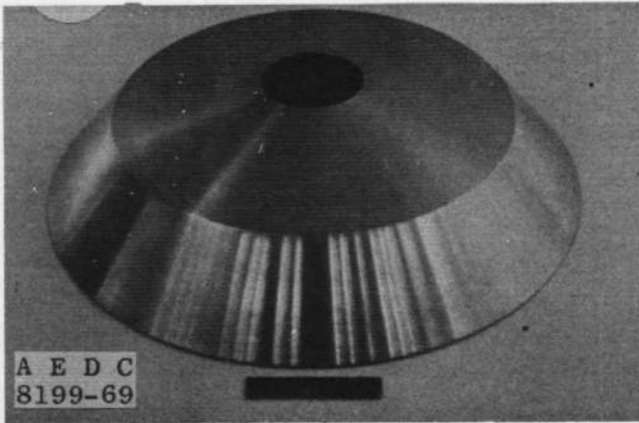
Config. 6B0M



Config. 6B2M

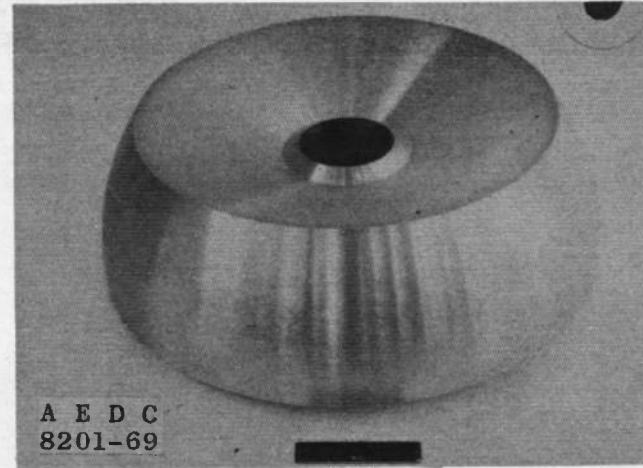
b. $\theta_c = 60$ deg

Fig. 3 Photographs of Martin Models

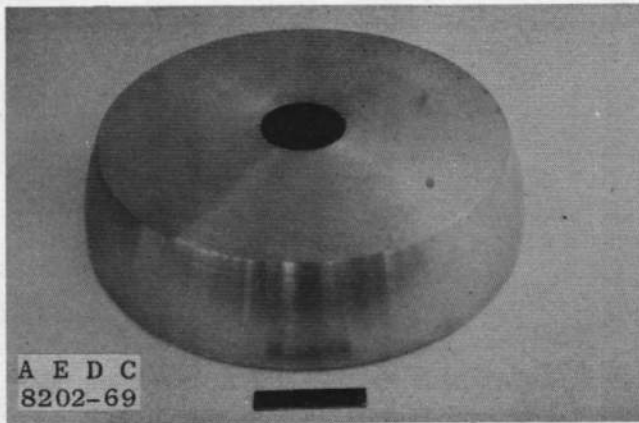


C = 1 $\theta_c = 70\text{-deg}$

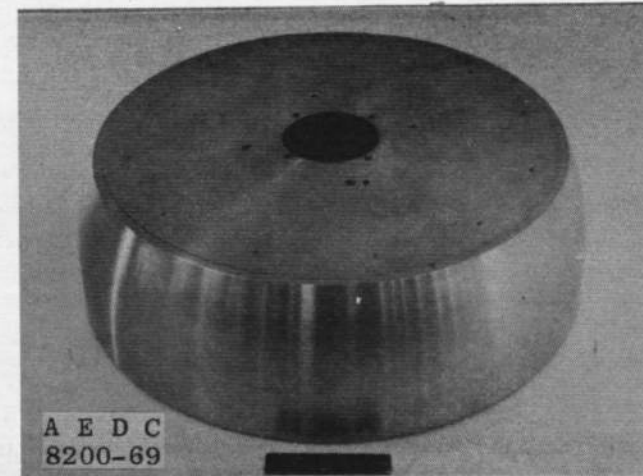
C = 2 $\theta_c = 60\text{-deg}$



C = 3

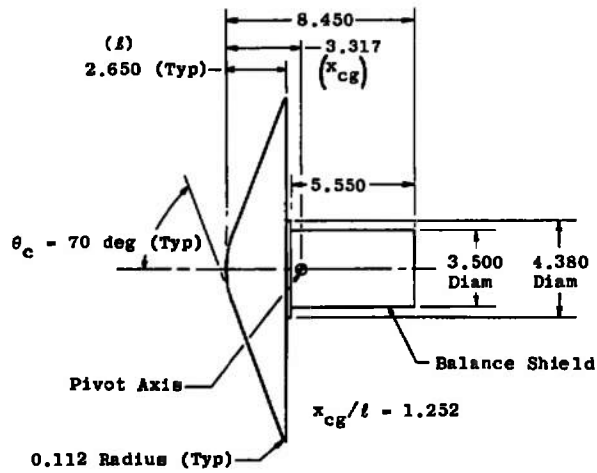


C = 4

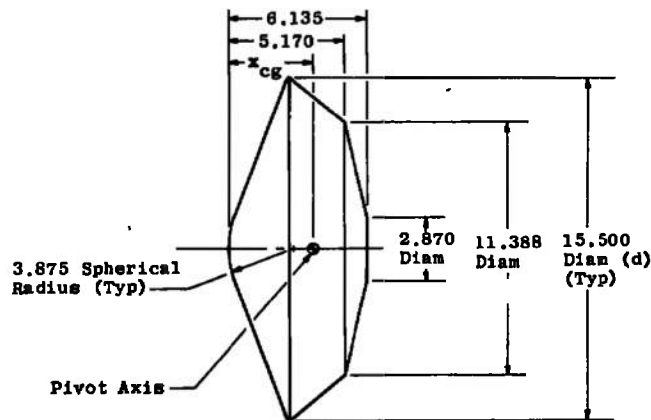


C = 5

Fig. 4 Photographs of Martin Base Fairings



a. Config. 720M

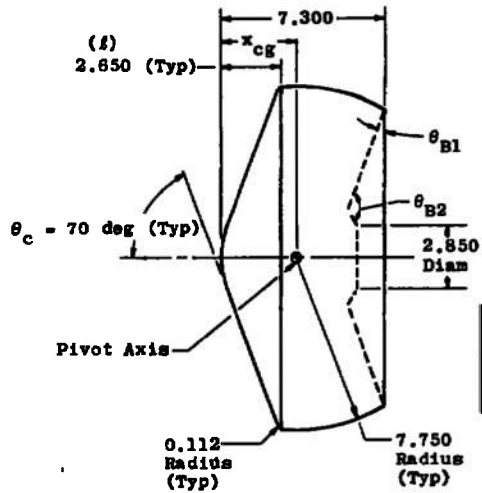


All Dimensions in Inches

Config.	A	B	C	x_{cg} , in.	x_{cg}/l
711M	70	1	1	2.650	1.000
721M	70	2	1	3.317	1.252
731M	70	3	1	3.782	1.428

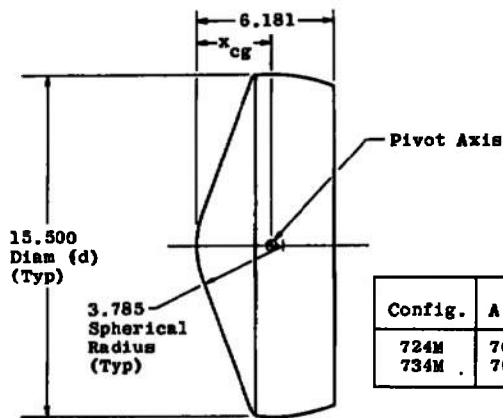
b. Config. 7B1M

Fig. 5 Model Geometry (Martin)



Config.	A	B	C	x_{cg} , in.	x_{cg}/l	θ_{B1} , deg	θ_{B2} , deg
723M	70	2	3	3.317	1.252	20	130
735M	70	3	5	3.782	1.428	0	180

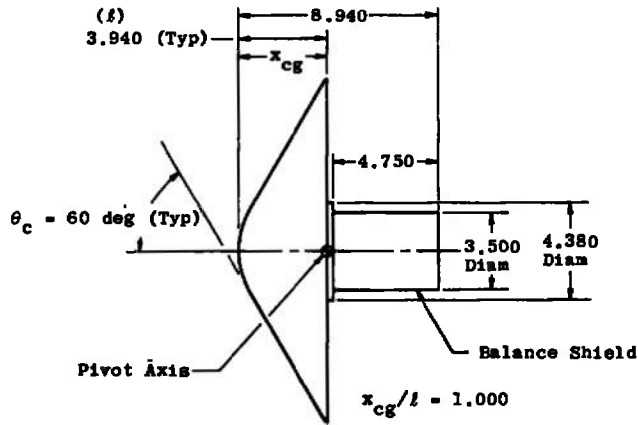
c. Config. 7BCM



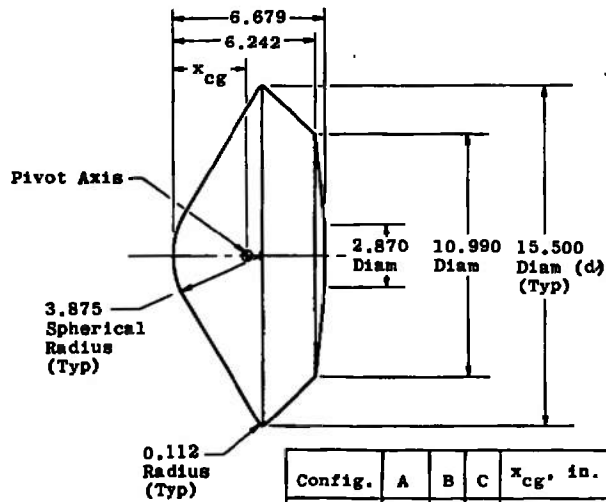
Config.	A	B	C	x_{cg} , in.	x_{cg}/l
724M	70	2	4	3.317	1.252
734M	70	3	4	3.782	1.428

All Dimensions in Inches

d. Config. 7B4M
Fig. 5 Continued



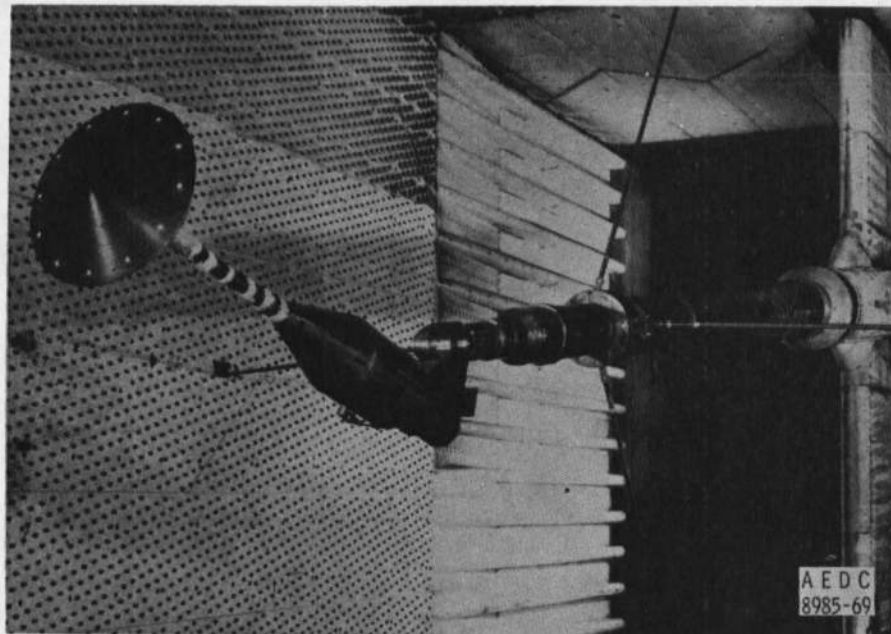
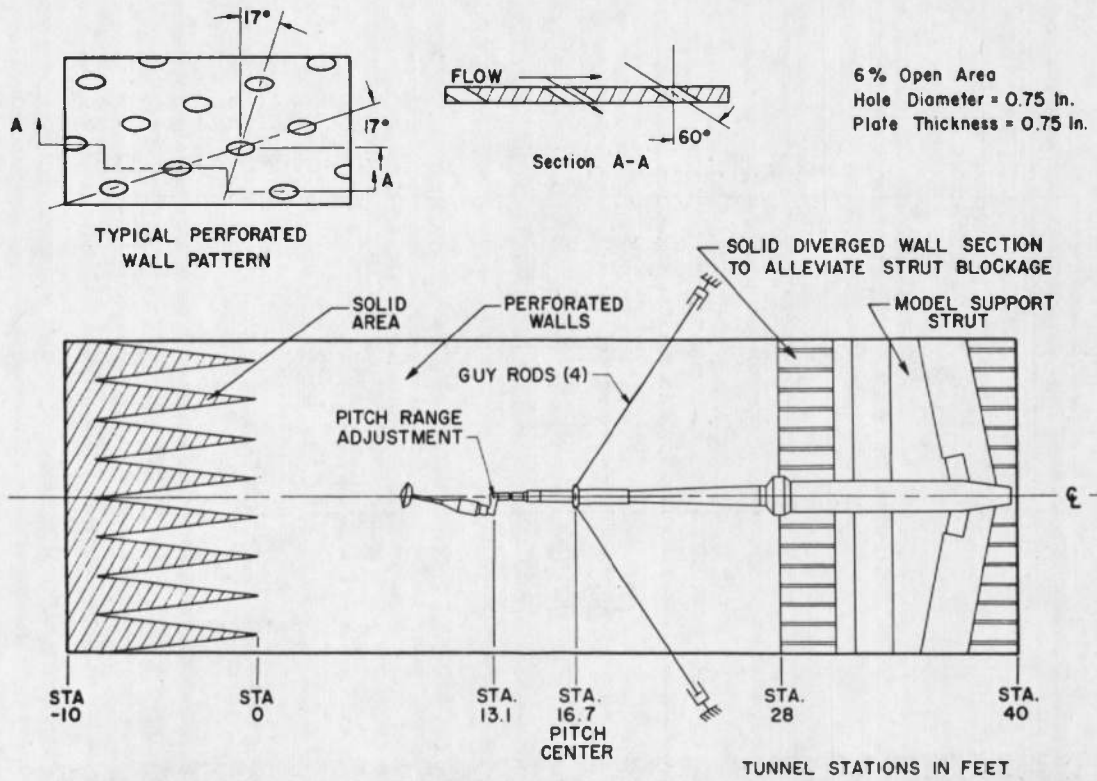
e. Config. 620M



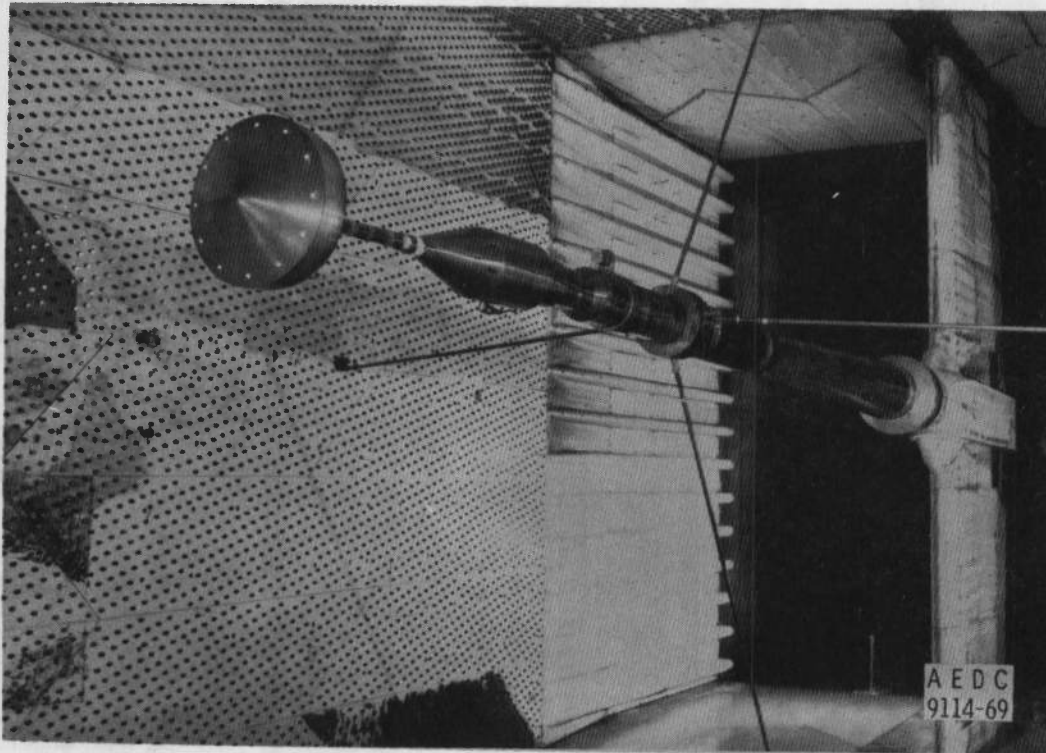
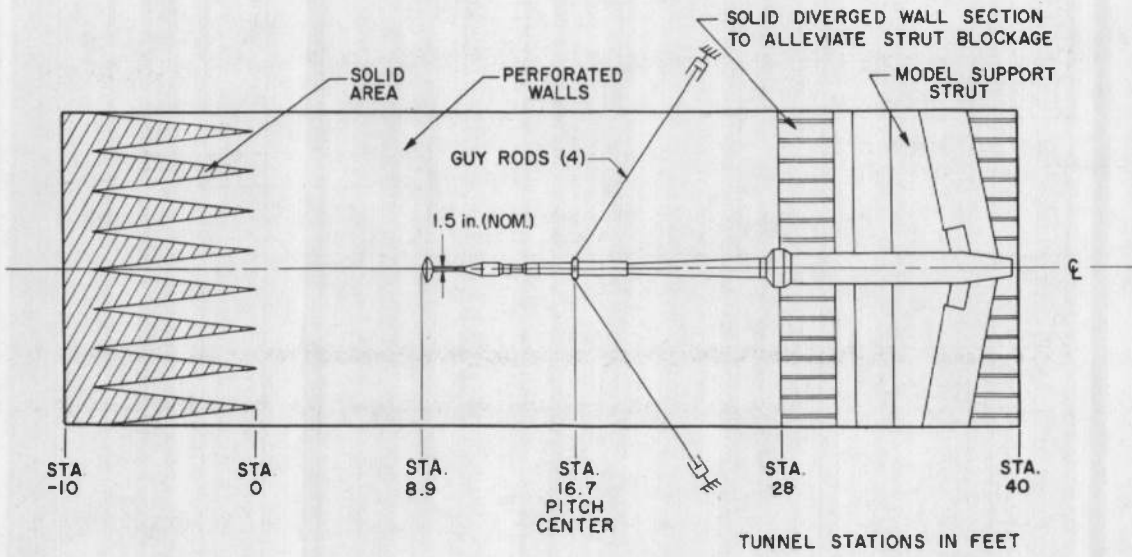
All Dimensions in Inches

Config.	A	B	C	x_{cg} , in.	x_{cg}/l
612M	60	1	2	3.273	0.831
622M	60	2	2	3.940	1.000

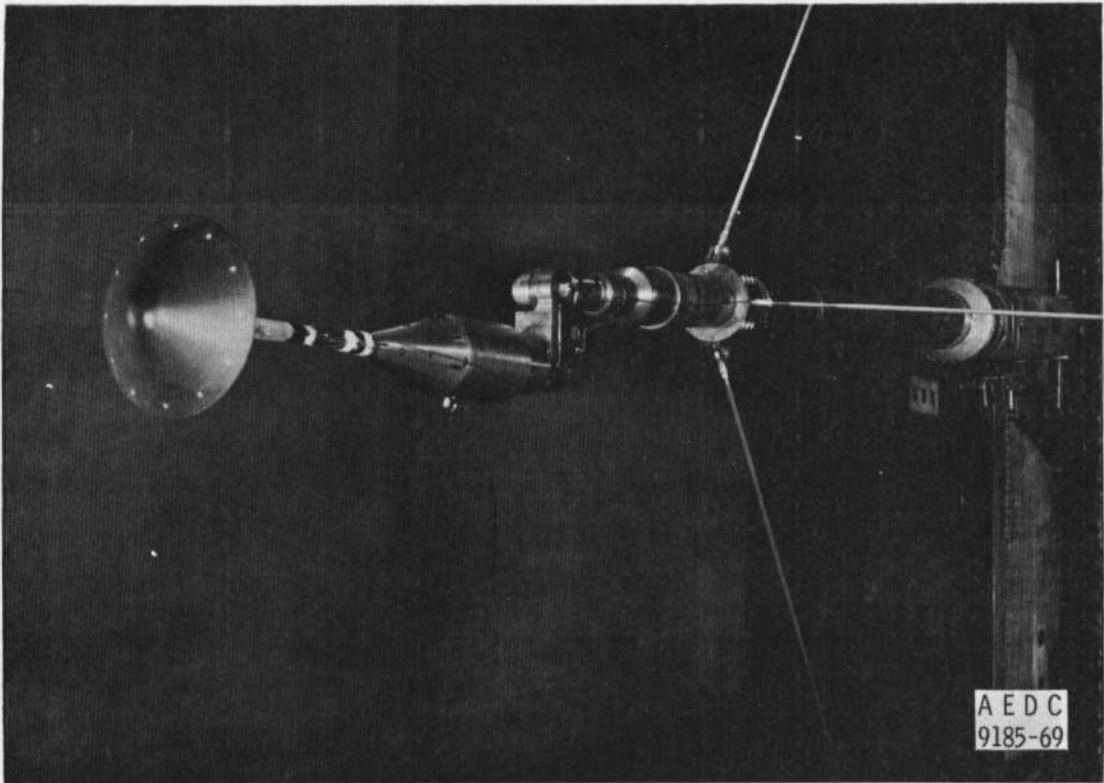
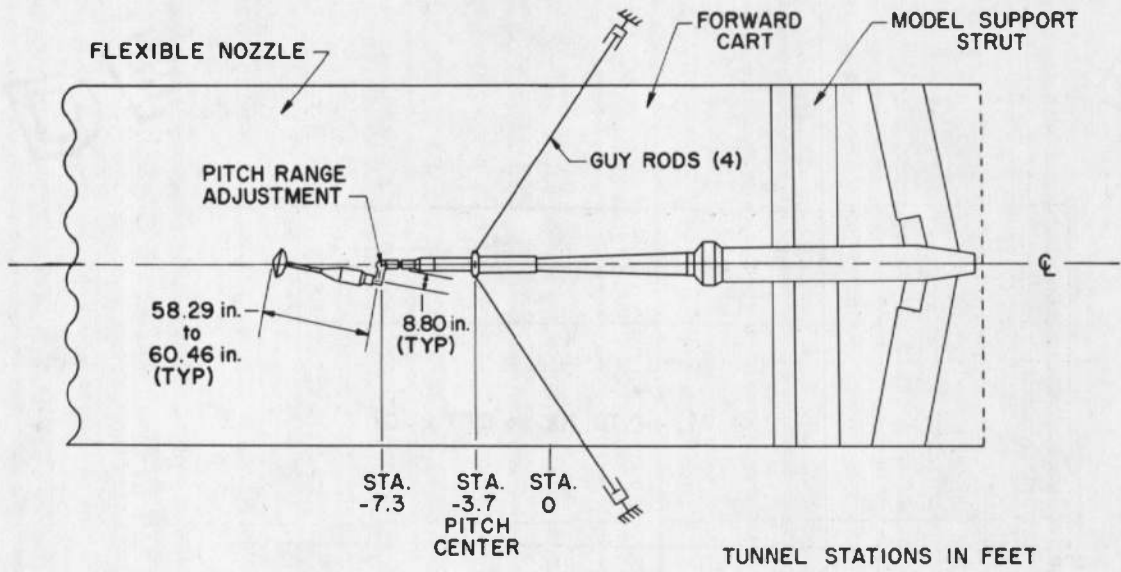
f. Config. 6B2M
Fig. 5 Concluded



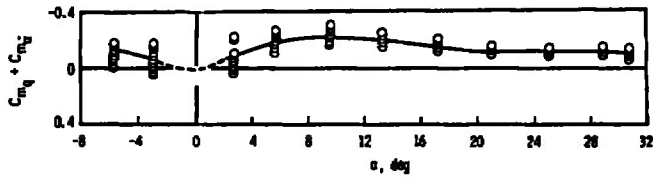
a. Bent Sting Support (16-T)
Fig. 6 Installation Photographs and Details



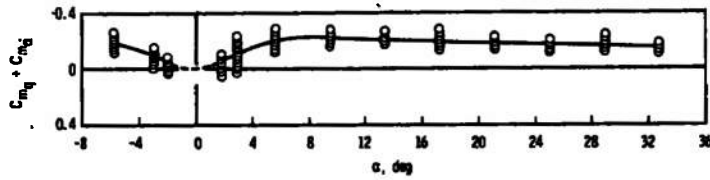
b. Straight Sting Support (16-T)
Fig. 6 Continued



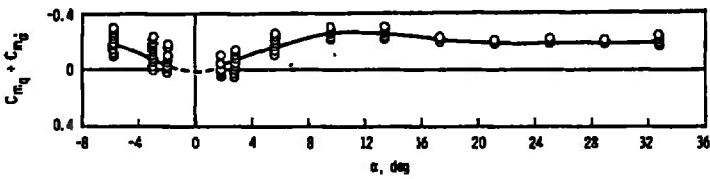
c. Bent Sting Support (16-S)
Fig. 6 Concluded



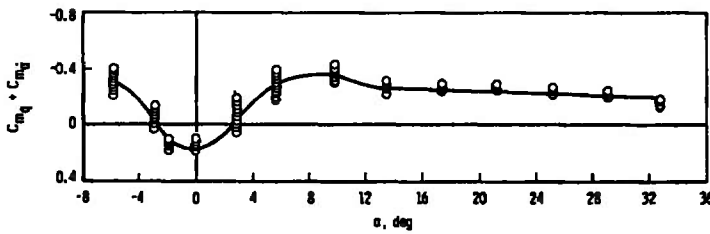
a. $M_\infty = 0.70, Re_d \approx 0.87 \times 10^6$



b. $M_\infty = 0.80, Re_d \approx 0.79 \times 10^6$

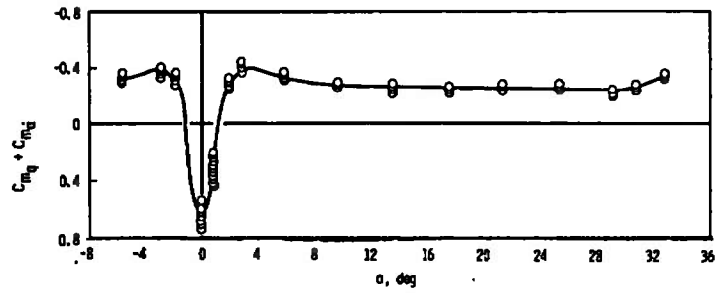


c. $M_\infty = 0.90, Re_d \approx 0.73 \times 10^6$

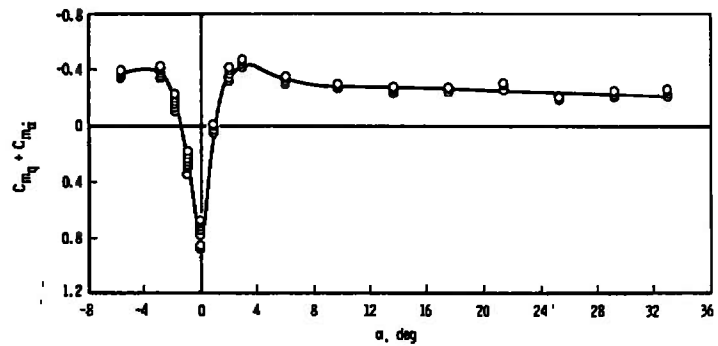


d. $M_\infty = 1.00, Re_d \approx 0.69 \times 10^6$

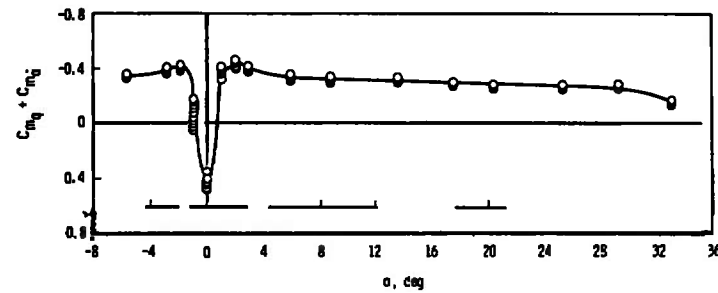
Fig. 7 Damping-in-Pitch Derivatives as a Function of Angle of Attack, Config. 721M, $x_{cg}/l = 1.252$



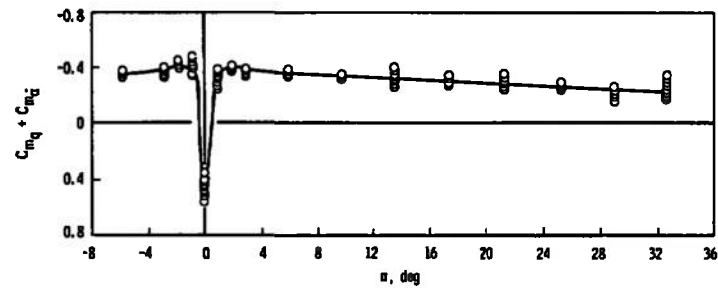
e. $M_\infty = 1.10, Re_d \approx 0.65 \times 10^6$



f. $M_\infty = 1.20, Re_d \approx 0.63 \times 10^6$

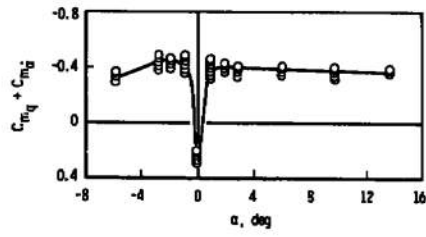


g. $M_\infty = 1.40, Re_d \approx 0.60 \times 10^6$

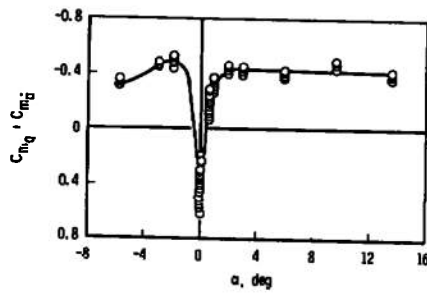


h. $M_\infty = 1.53, Re_d \approx 0.58 \times 10^6$

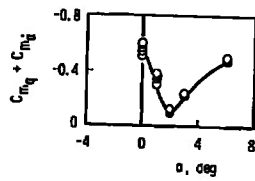
Fig. 7 Continued



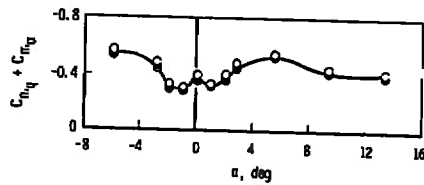
i. $M_\infty = 1.60, Re_d \approx 0.58 \times 10^6$



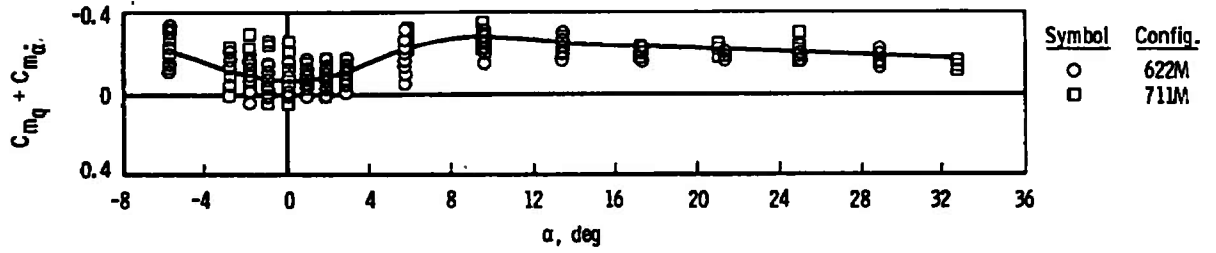
j. $M_\infty = 1.90, Re_d \approx 0.58 \times 10^6$



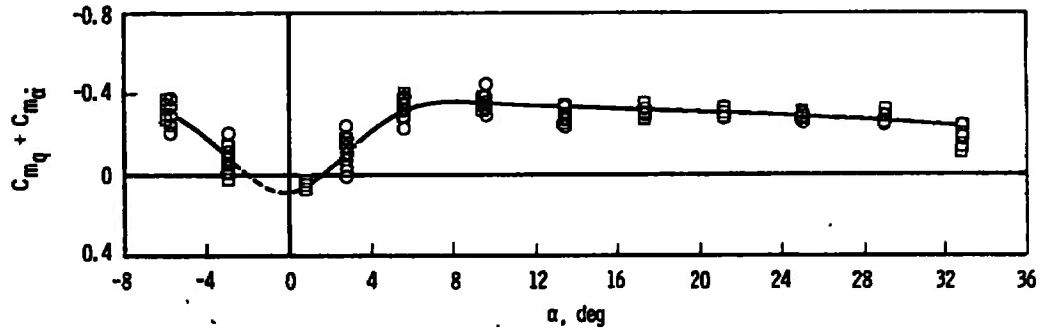
k. $M_\infty = 2.65, Re_d \approx 0.69 \times 10^6$



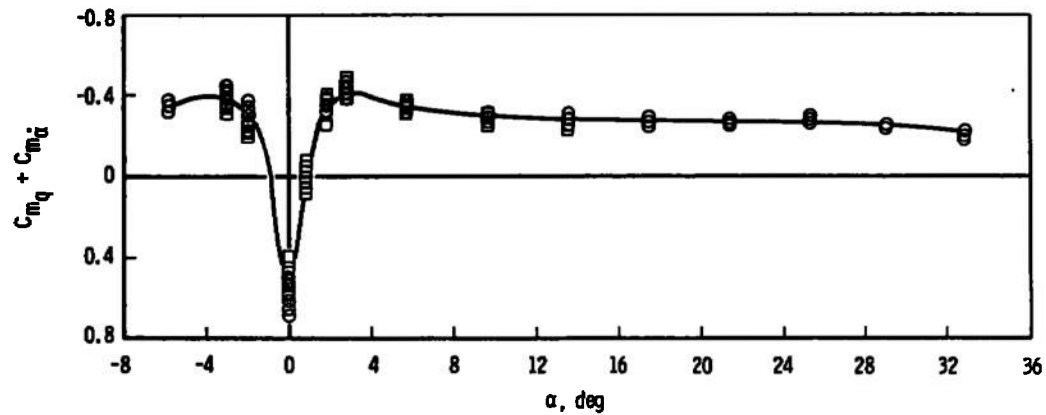
l. $M_\infty = 3.00, Re_d \approx 0.73 \times 10^6$
 Fig. 7. Concluded



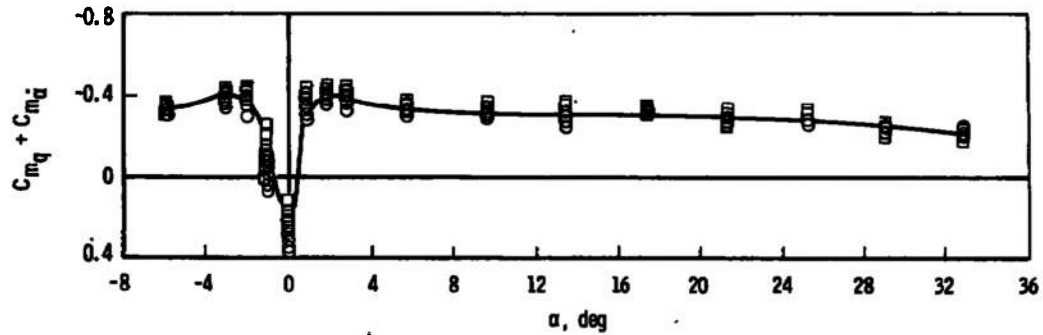
a. $M_\infty = 0.80, Re_d \approx 0.79 \times 10^6$



b. $M_\infty = 1.00, Re_d \approx 0.69 \times 10^6$



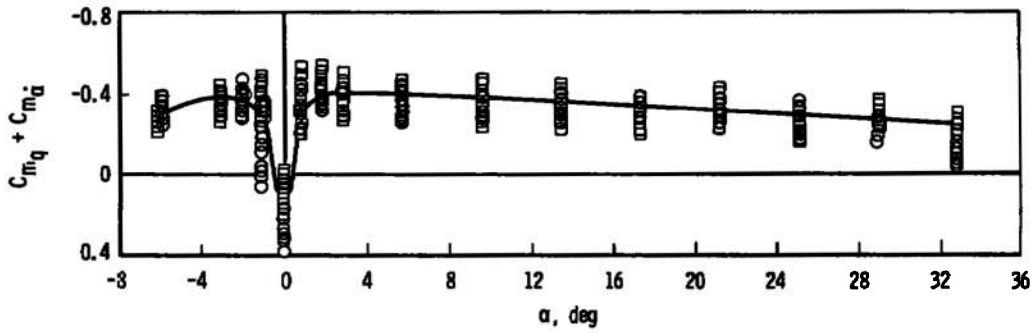
c. $M_\infty = 1.20, Re_d \approx 0.63 \times 10^6$



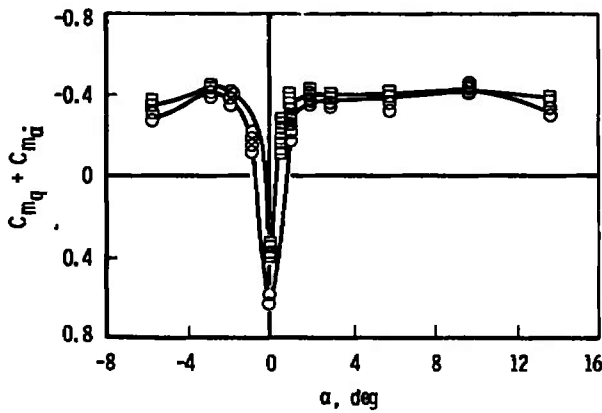
d. $M_\infty = 1.40, Re_d \approx 0.59 \times 10^6$

Fig. 8 Damping-in-Pitch Derivatives as a Function of Angle of Attack, Configs. 622M and 711M, $x_{cg}/\ell = 1.000$

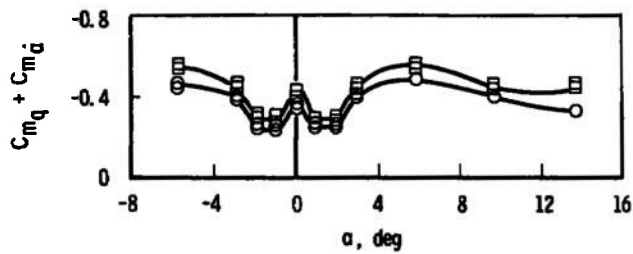
Symbol	Config.
○	622M
□	711M



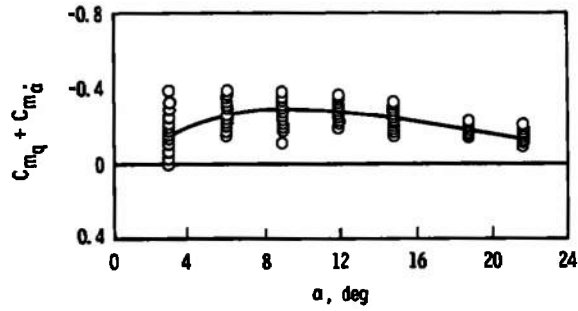
e. $M_\infty = 1.60, Re_d \approx 0.58 \times 10^6$



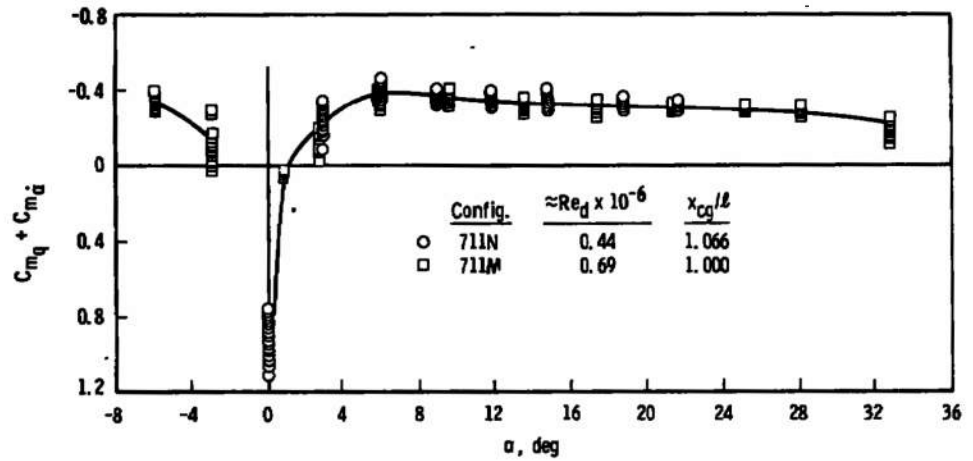
f. $M_\infty = 1.90, Re_d \approx 0.58 \times 10^6$



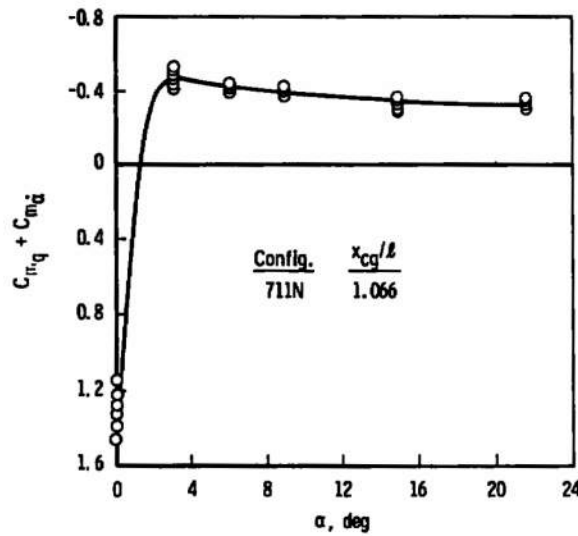
g. $M_\infty = 3.00, Re_d \approx 0.74 \times 10^6$
 Fig. 8 Concluded



a. $M_\infty = 0.60, Re_d \approx 0.63 \times 10^6$

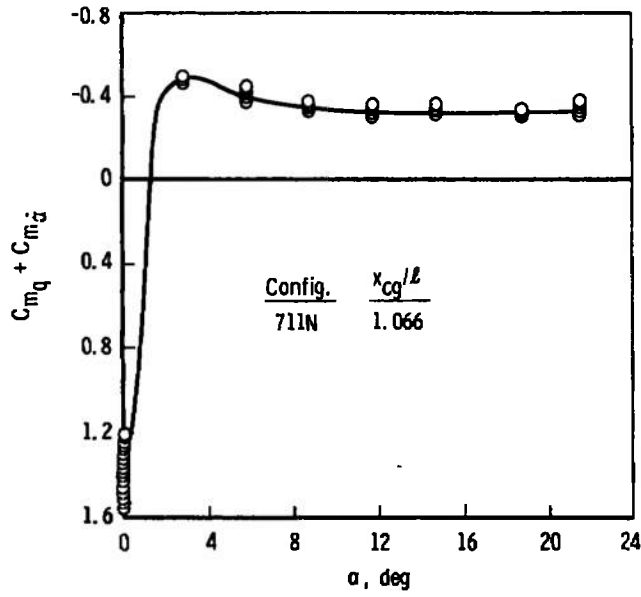


b. $M_\infty = 1.00$

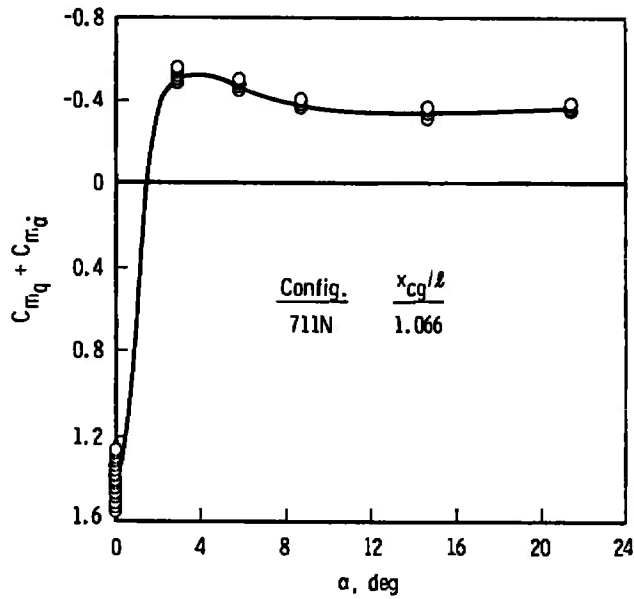


c. $M_\infty = 1.15, Re_d \approx 0.41 \times 10^6$

Fig. 9 Damping-in-Pitch Derivatives as a Function of Angle of Attack, Configs. 711N and 711M

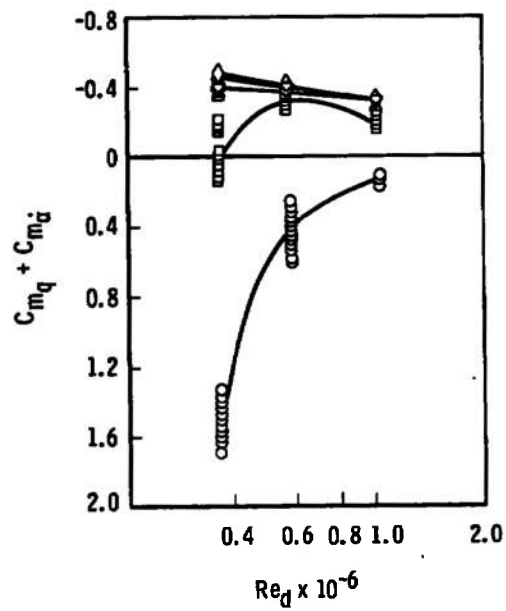


d. $M_\infty = 1.30, Re_d \approx 0.39 \times 10^6$

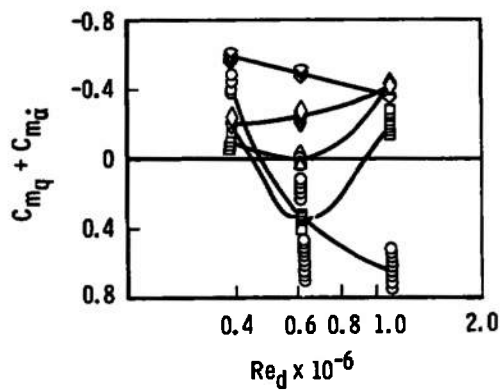


e. $M_\infty = 1.50, Re_d \approx 0.58 \times 10^6$

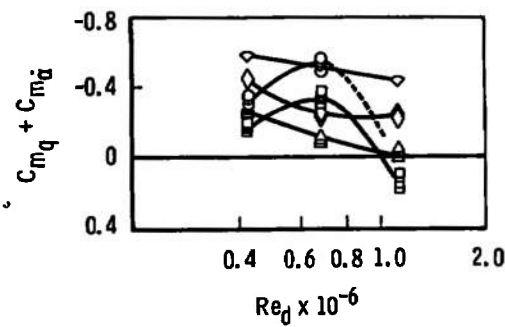
Fig. 9 Concluded



a. $M_\infty = 1.90$



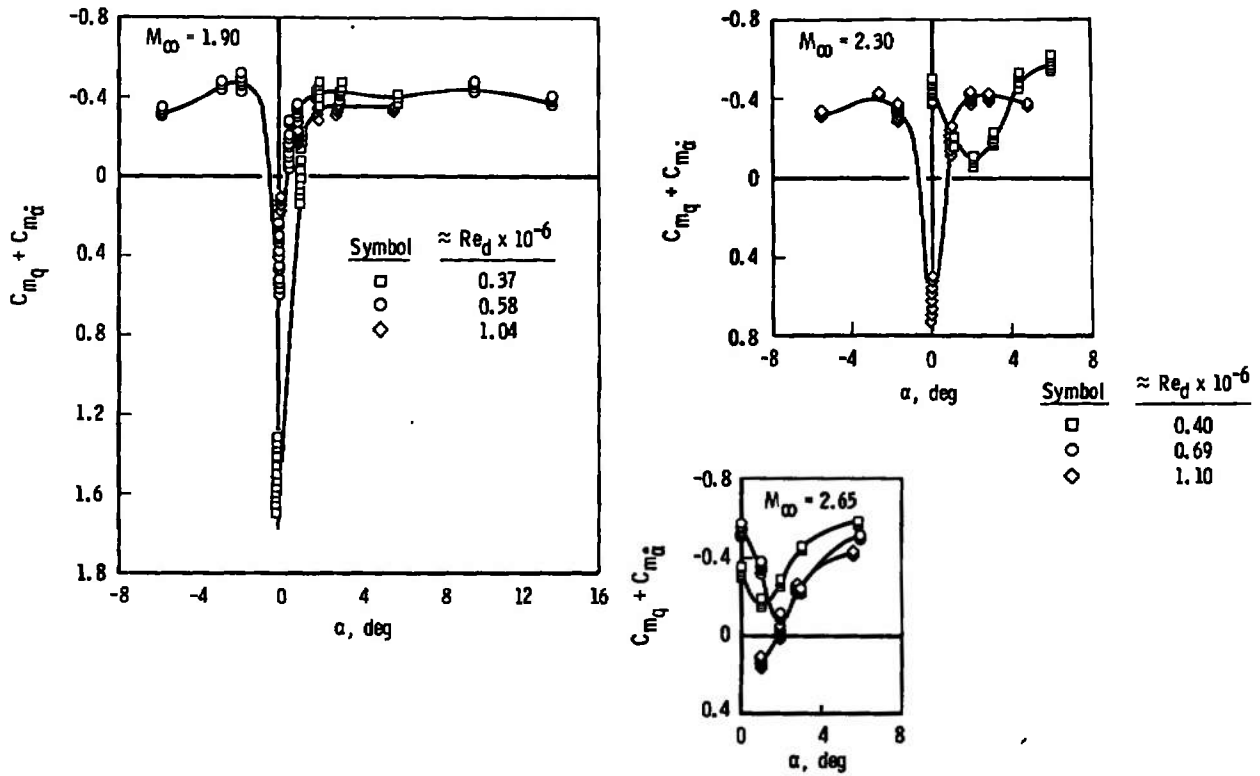
b. $M_\infty = 2.30$



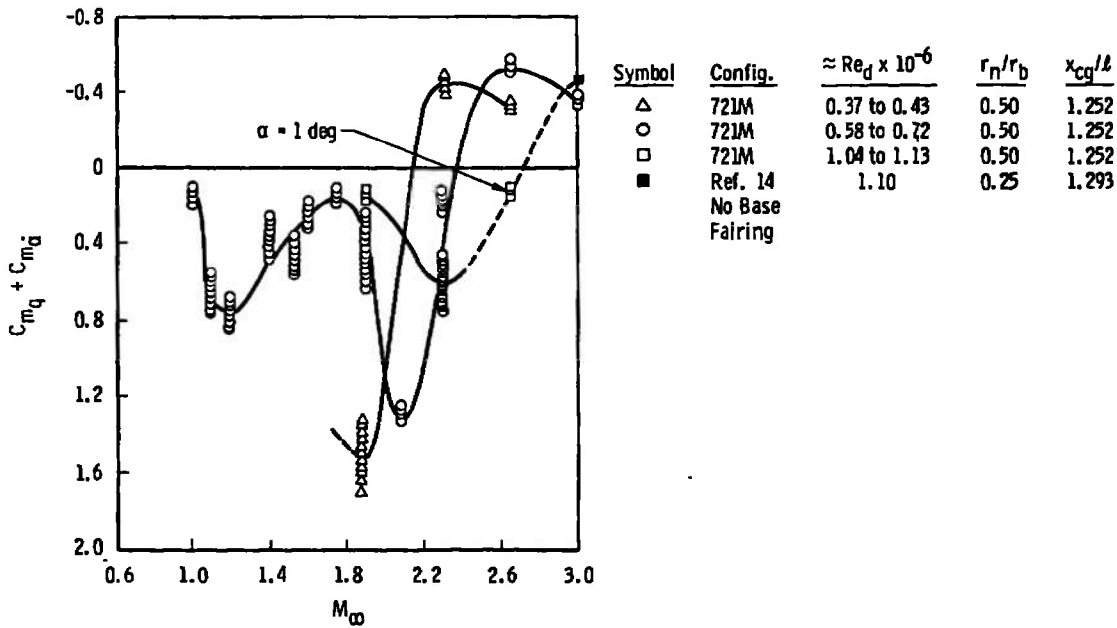
c. $M_\infty = 2.65$

Symbol	$\approx \alpha$, deg
○	0
□	1
△	1.9
◇	2.9
◊	5.8

Fig. 10 Damping-in-Pitch Derivatives as a Function of Reynolds Number, Config. 721M, $x_{cg}/l = 1.252$

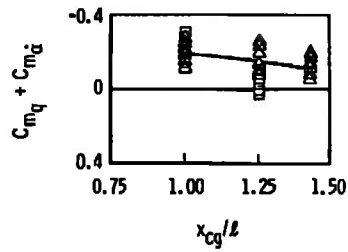


a. Damping Trends as Function of Angle of Attack

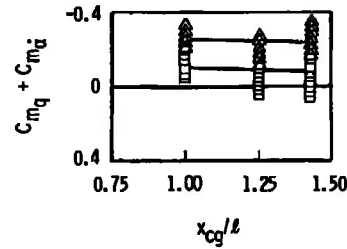


b. Damping Trends as a Function of Mach Number, $\alpha = 0$

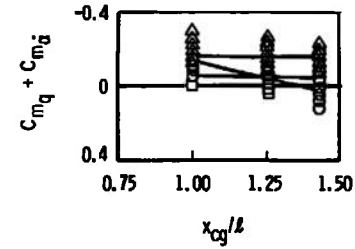
Fig. 11 Effects of Reynolds Number, Config. 721M, $x_{cg}/l = 1.252$



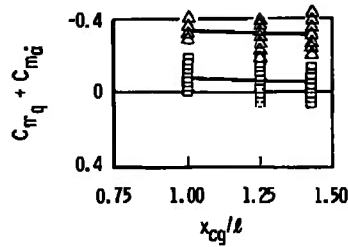
a. $M_\infty = 0.70, Re_d \approx 0.87 \times 10^6$



b. $M_\infty = 0.80, Re_d \approx 0.79 \times 10^6$

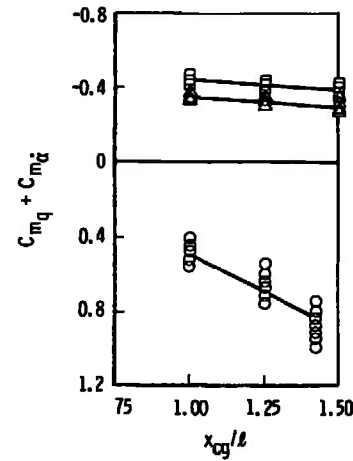


c. $M_\infty = 0.90, Re_d \approx 0.73 \times 10^6$



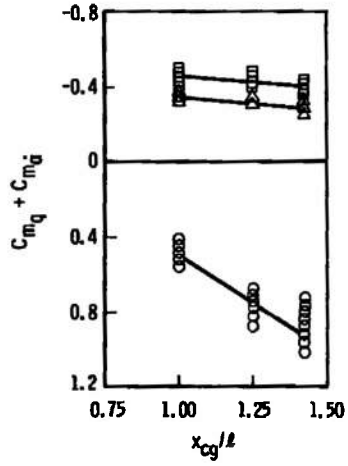
d. $M_\infty = 1.00, Re_d \approx 0.69 \times 10^6$

Symbol	$\approx \alpha, \text{ deg}$
○	0
□	2.9
△	5.8

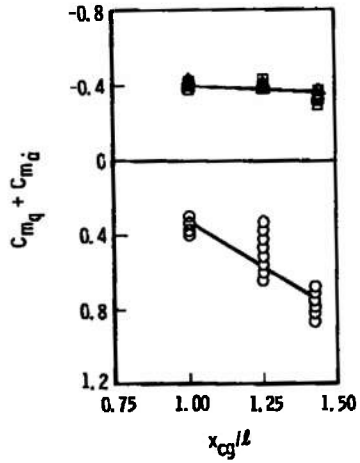


e. $M_\infty = 1.10, Re_d \approx 0.66 \times 10^6$

Fig. 12 Damping-in-Pitch Derivatives as a Function of Center-of-Gravity Location, Config. 7B1M

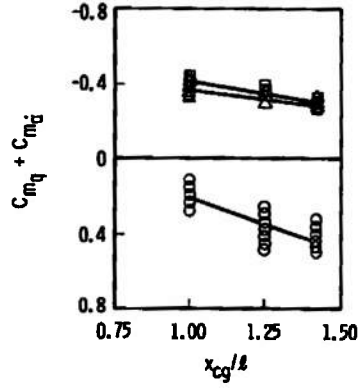


f. $M_\infty = 1.20,$
 $Re_d \approx 0.62 \times 10^6$

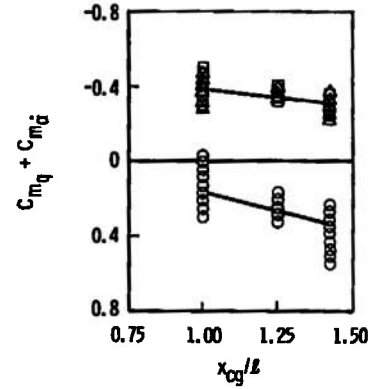


i. $M_\infty = 1.90,$
 $Re_d \approx 0.58 \times 10^6$

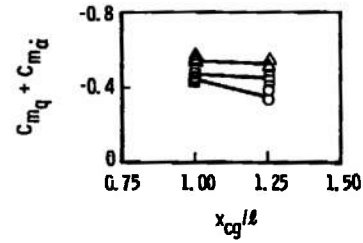
Symbol	$\approx \alpha, \text{ deg}$
○	0
□	2.9
△	5.8



g. $M_\infty = 1.40,$
 $Re_d \approx 0.59 \times 10^6$

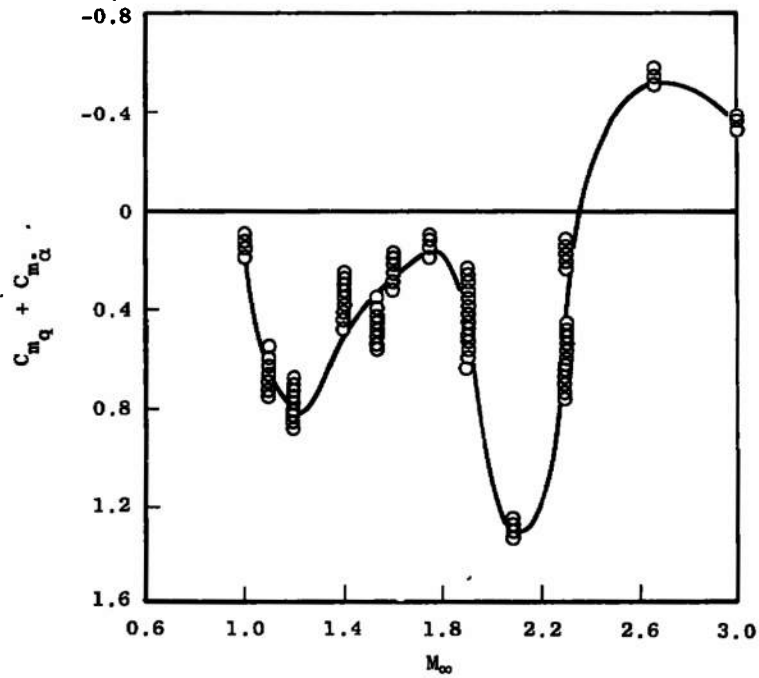


h. $M_\infty = 1.60,$
 $Re_d \approx 0.58 \times 10^6$

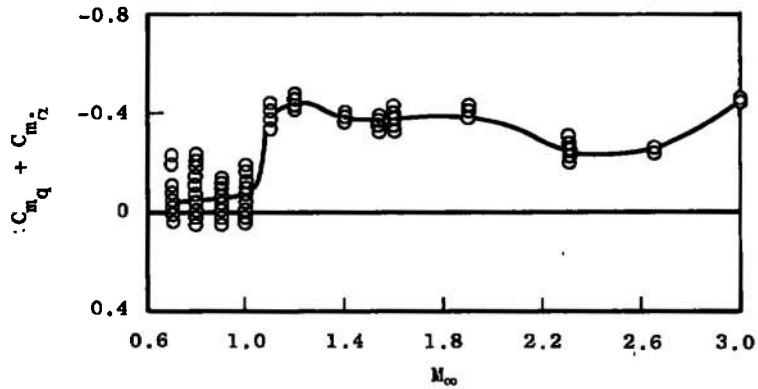


j. $M_\infty = 3.00,$
 $Re_d \approx 0.73 \times 10^6$

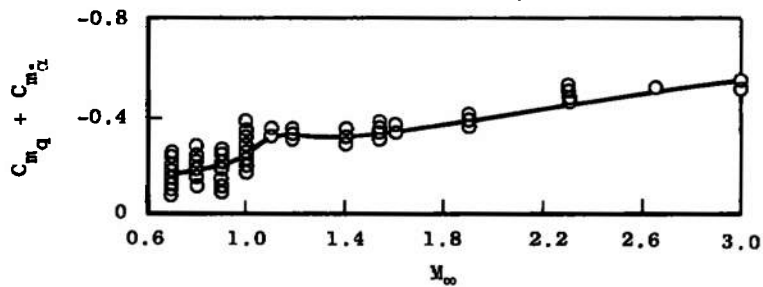
Fig. 12 Concluded



a. $\alpha = 0$, $Re_d \approx 0.58 \times 10^6$ to 0.72×10^6

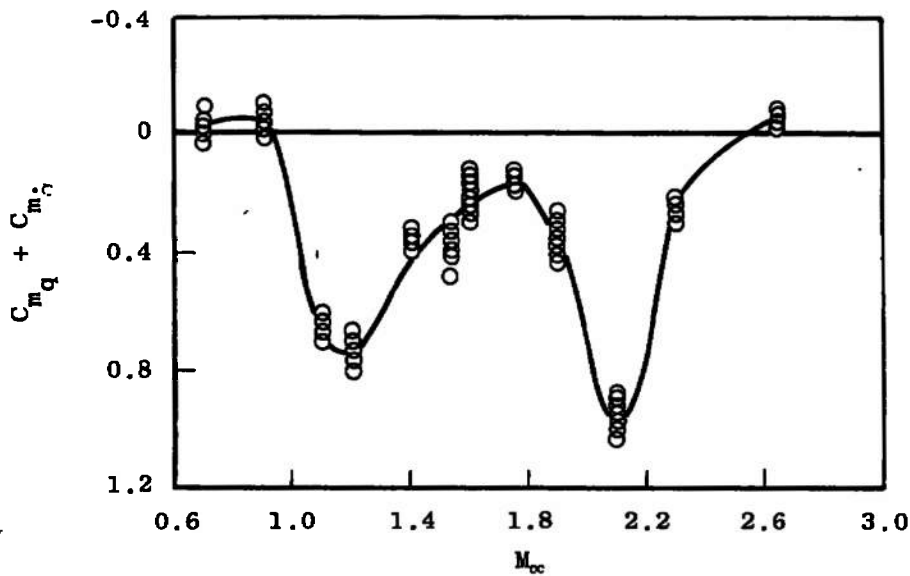


b. $\alpha \approx 2.9$, $Re_d \approx 0.58 \times 10^6$ to 0.88×10^6

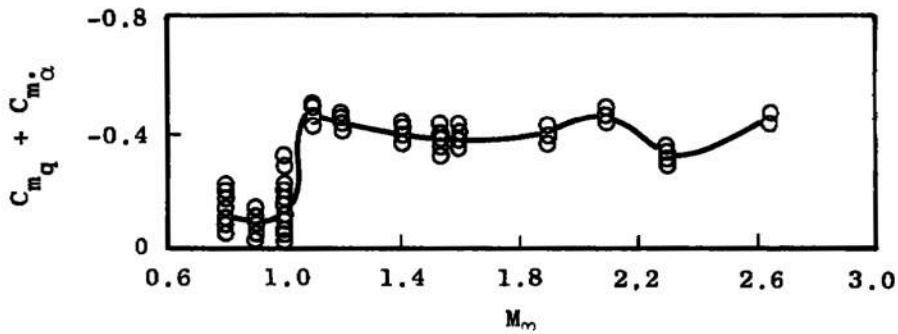


c. $\alpha \approx 5.8$ deg, $Re_d \approx 0.58 \times 10^6$ to 0.88×10^6

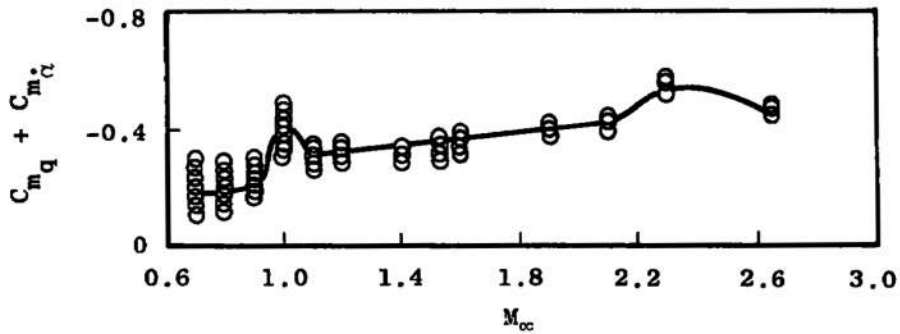
Fig. 13 Damping-in-Pitch Derivatives as a Function of Mach Number, Config. 721M, $x_{cg}/\bar{c} = 1.252$



a. $\alpha = 0$

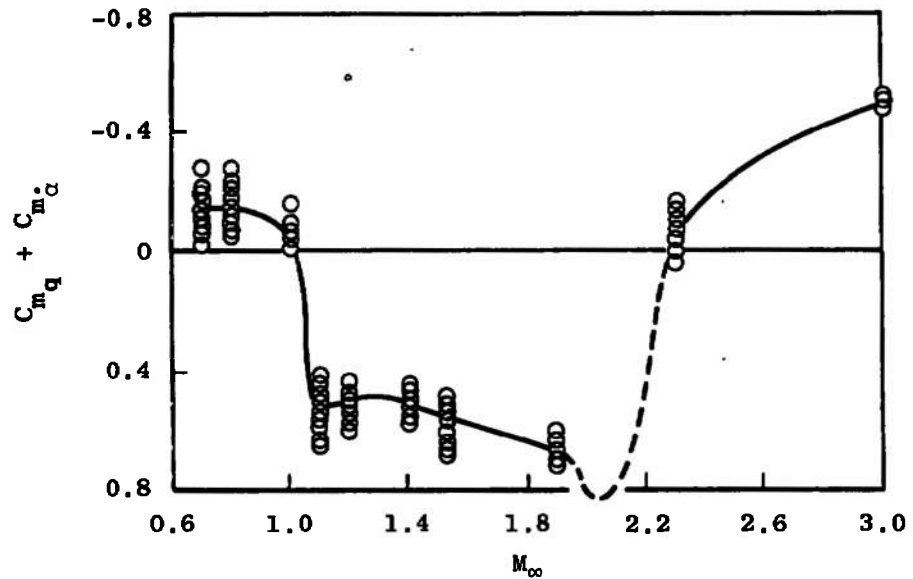


b. $\alpha \approx 2.9$ deg

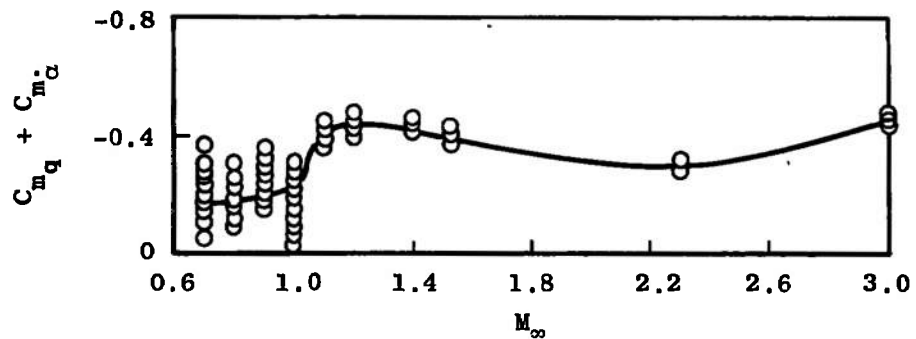


c. $\alpha \approx 5.8$ deg

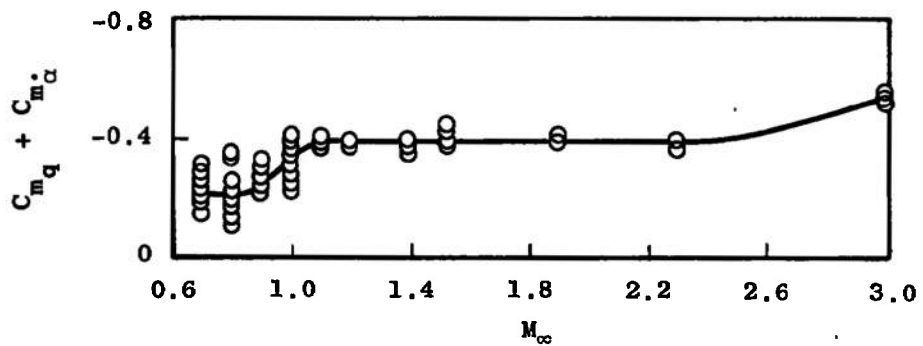
Fig. 14 Damping-in-Pitch Derivatives as a Function of Mach Number, Config. 724M, $x_{cg}/l = 1.252$, $Re_d \approx 0.57 \times 10^6$ to 0.87×10^6



a. $\alpha = 0$

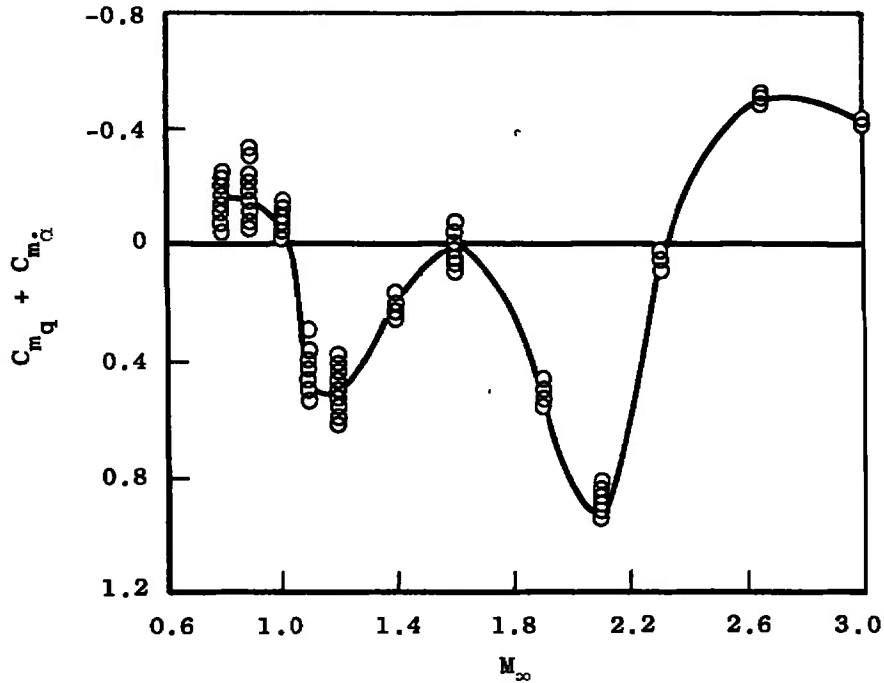


b. $\alpha \approx 2.9$ deg

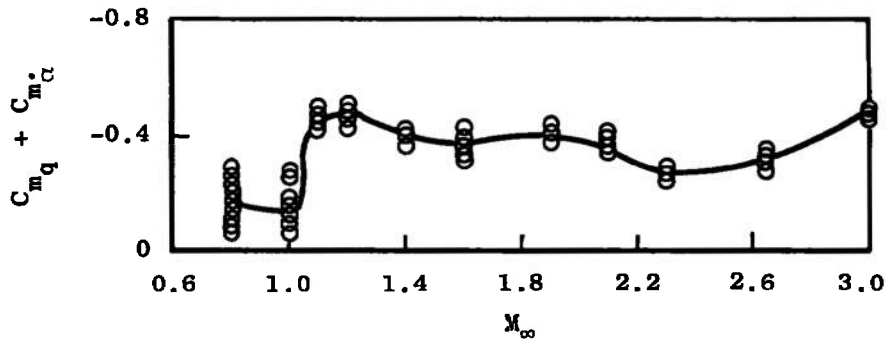


c. $\alpha \approx 5.8$ deg

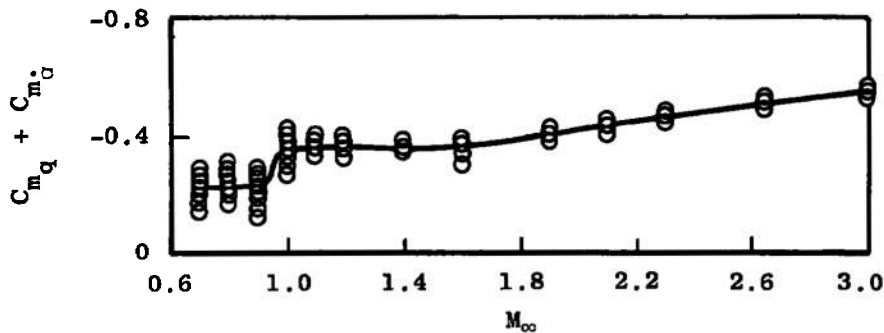
Fig. 15 Damping-in-Pitch Derivatives as a Function of Mach Number, Config. 720M, $x_{c_g}/\ell = 1.252$, $Re_d \approx 0.58 \times 10^6$ to 0.88×10^6



a. $\alpha = 0$, $Re_d \approx 0.57 \times 10^6$ to 0.79×10^6

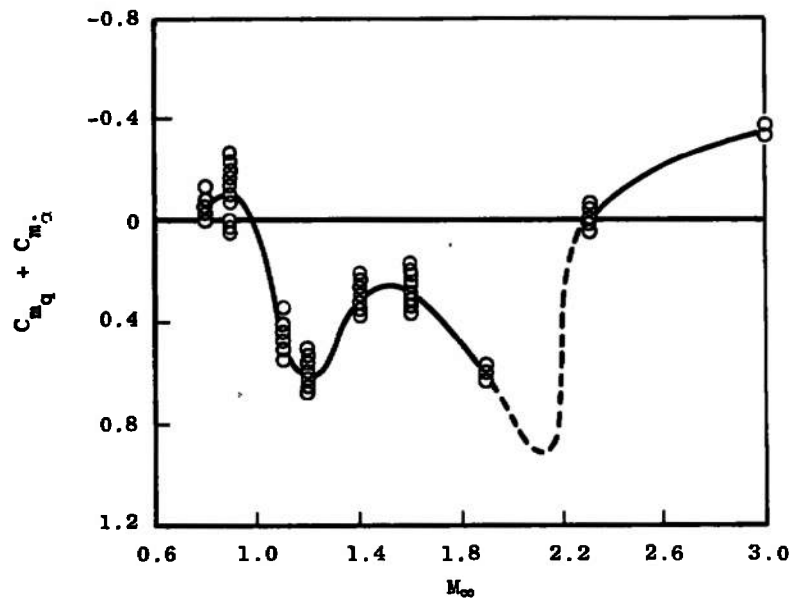


b. $\alpha \approx 2.9$ deg, $Re_d \approx 0.57 \times 10^6$ to 0.79×10^6

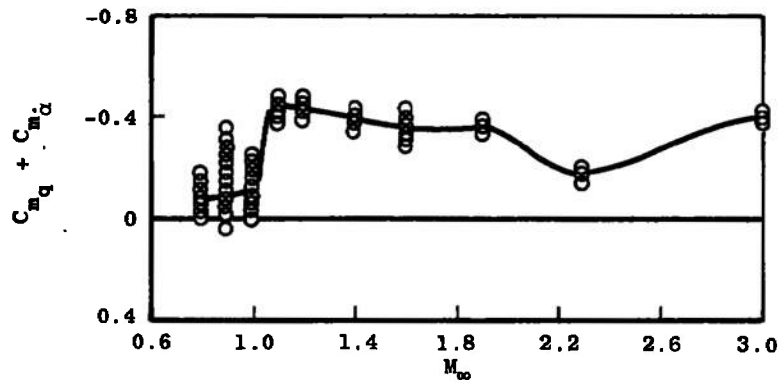


c. $\alpha \approx 5.8$ deg, $Re_d \approx 0.57 \times 10^6$ to 0.89×10^6

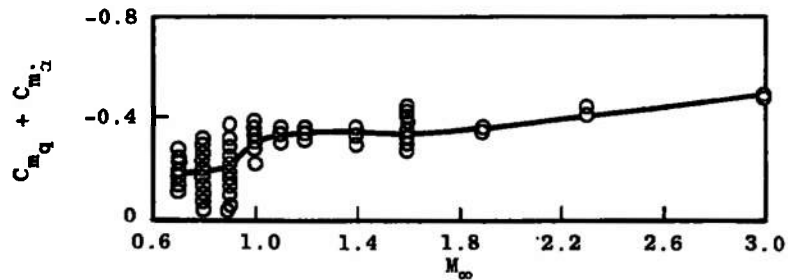
Fig. 16 Damping-in-Pitch Derivatives as a Function of Mach Number, Config. 612M, $x_{cg}/l = 0.831$



a. $\alpha = 0$, $Re_d \approx 0.58 \times 10^6$ to 0.79×10^6

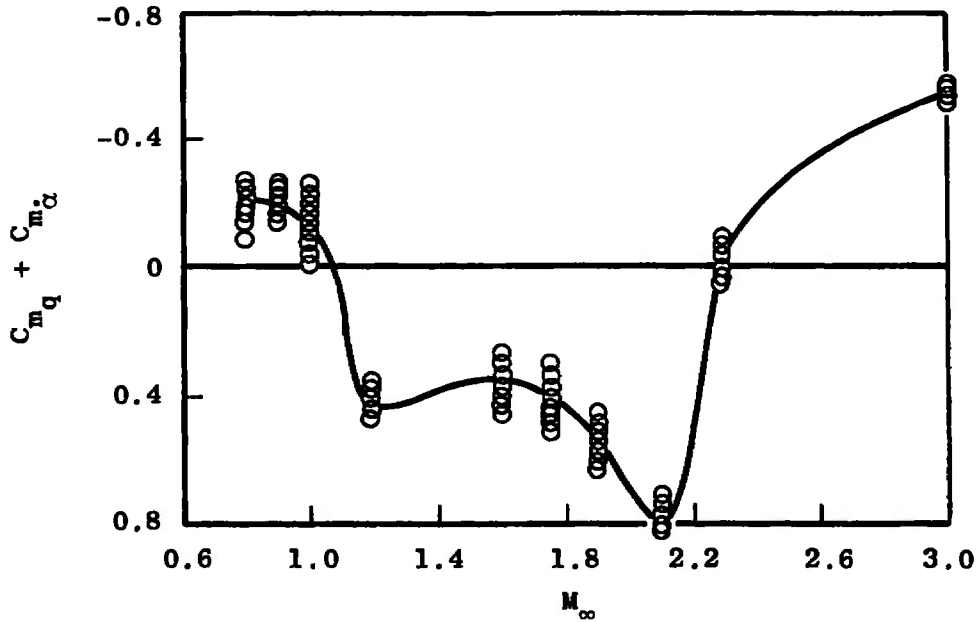


b. $\alpha \approx 2.9$ deg, $Re_d \approx 0.58 \times 10^6$ to 0.79×10^6

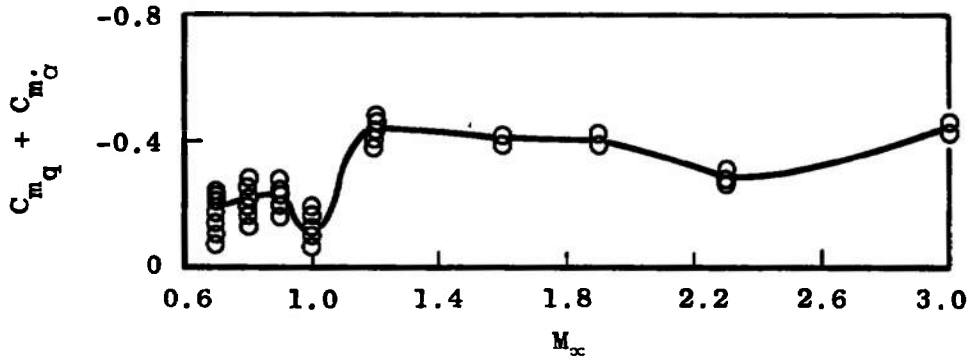


c. $\alpha \approx 5.8$ deg, $Re_d \approx 0.58 \times 10^6$ to 0.87×10^6

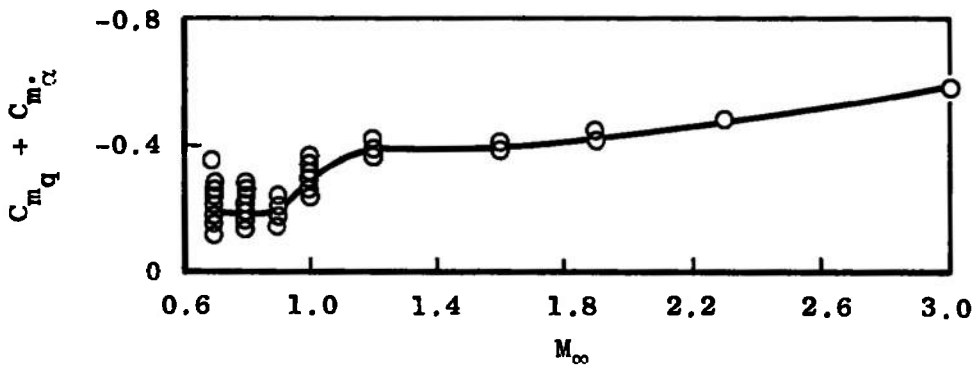
Fig. 17 Damping-in-Pitch Derivatives as a Function of Mach Number, Config. 622M, $x_{cg}/l = 1.000$



a. $\alpha = 0$, $Re_d \approx 0.58 \times 10^6$ to 0.79×10^6

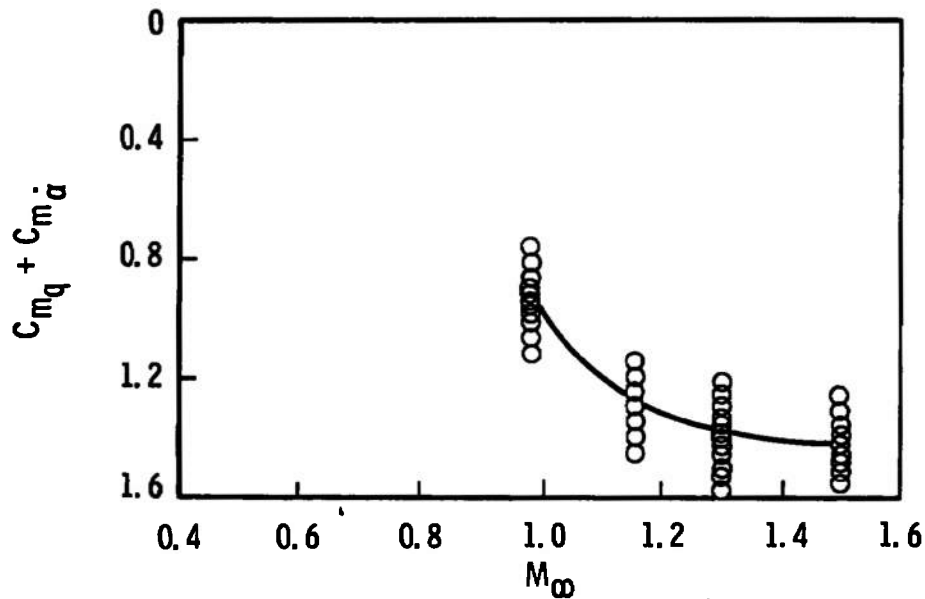


b. $\alpha \approx 2.9$ deg, $Re_d \approx 0.58 \times 10^6$ to 0.89×10^6

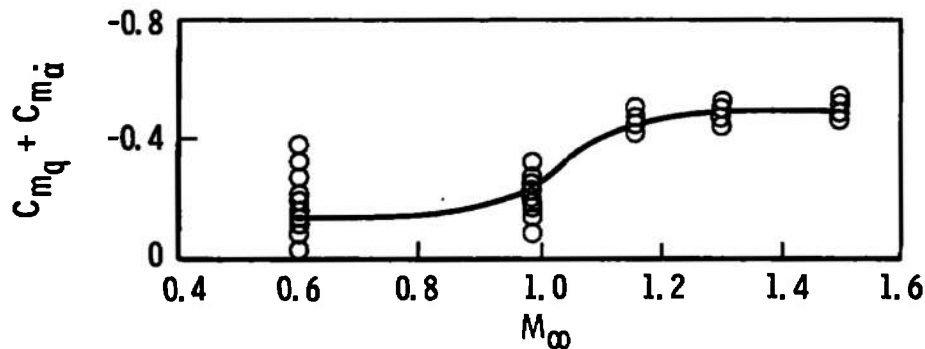


c. $\alpha \approx 5.8$ deg, $Re_d \approx 0.58 \times 10^6$ to 0.89×10^6

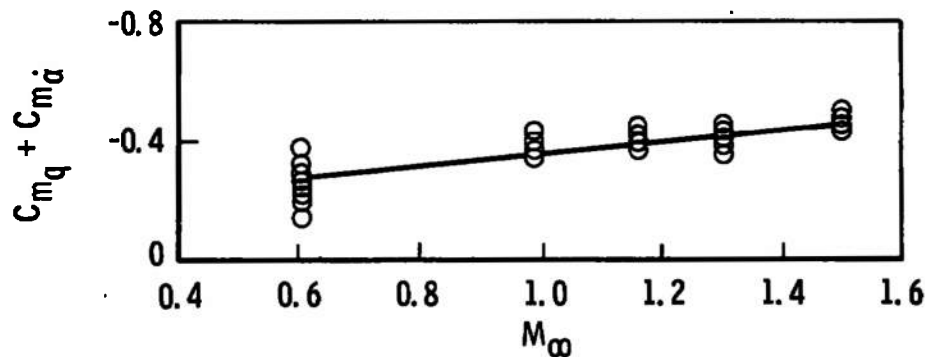
Fig. 18 Damping-in-Pitch Derivatives as a Function of Mach Number, Config. 620M
 $x_{cg}/l = 1.000$



a. $\alpha = 0$, $Re_d \approx 0.39 \times 10^6$ to 0.58×10^6

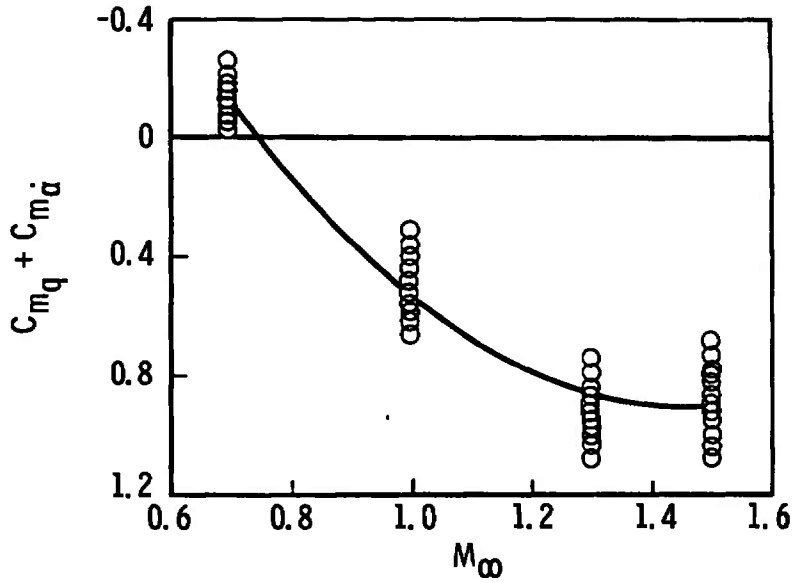


b. $\alpha \approx 2.9$ deg, $Re_d \approx 0.39 \times 10^6$ to 0.63×10^6

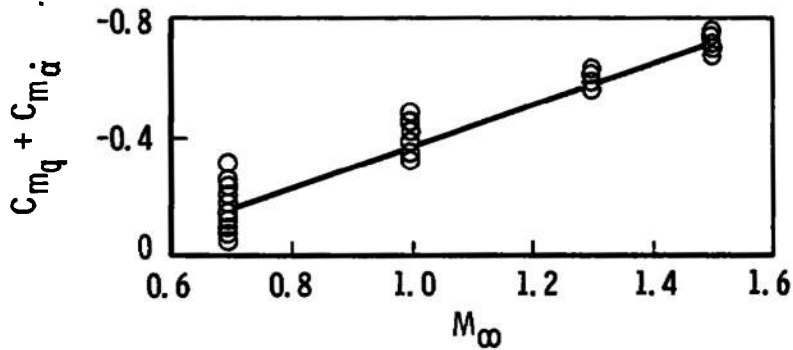


c. $\alpha \approx 5.8$ deg, $Re_d \approx 0.39 \times 10^6$ to 0.63×10^6

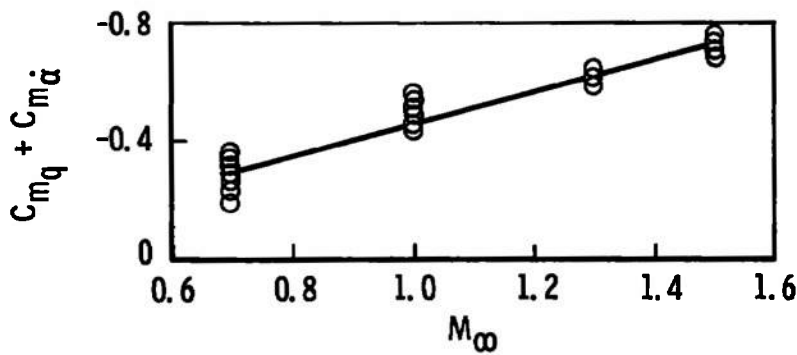
Fig. 19 Damping-in-Pitch Derivatives as a Function of Mach Number, Config. 711N, $x_{cg}/l = 1.066$



a. $\alpha = 0$



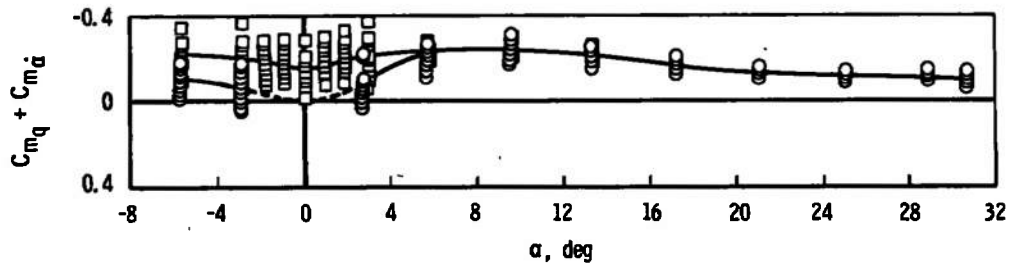
b. $\alpha \approx 2.9$ deg



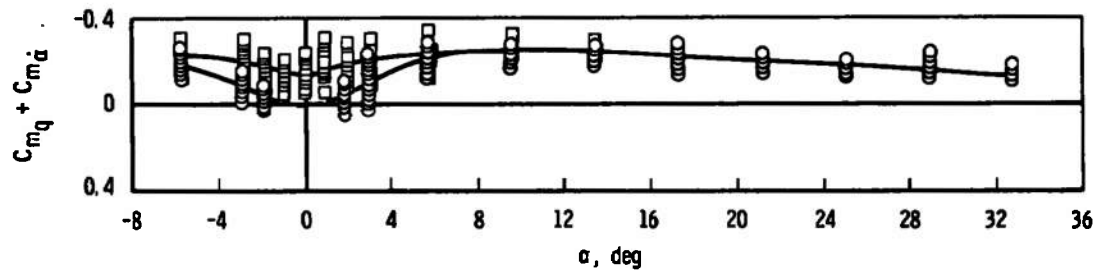
c. $\alpha \approx 5.8$ deg

Fig. 20 Damping-in-Pitch Derivatives as a Function of Mach Number, Config. 611N, $x_{cg}/l = 0.704$, $Re_d \approx 0.39 \times 10^6$ to 0.58×10^6

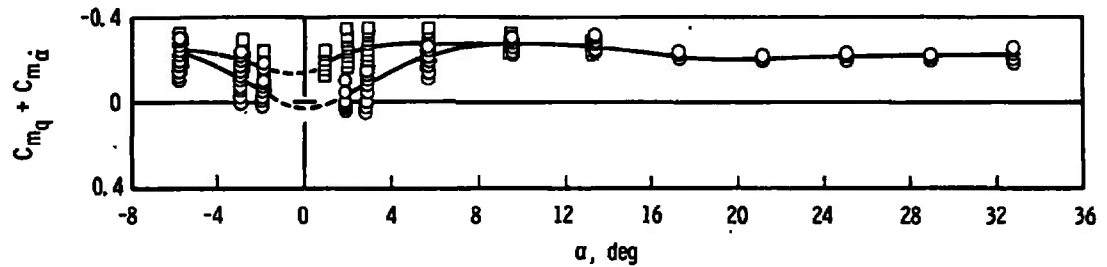
Symbol	Config.
○	721M
□	720M



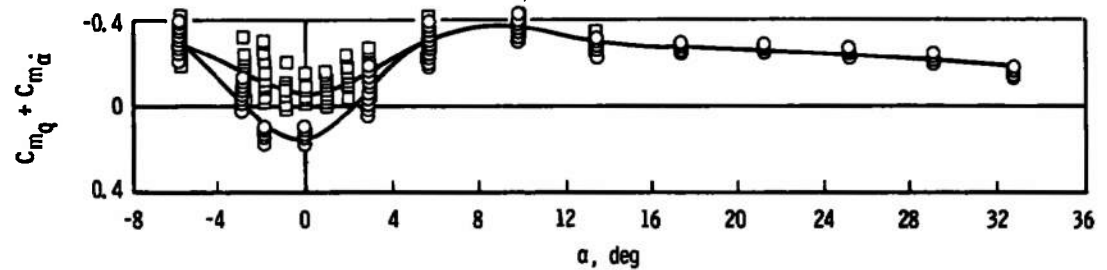
a. $M_\infty = 0.70, Re_d \approx 0.87 \times 10^6$



b. $M_\infty = 0.80, Re_d \approx 0.79 \times 10^6$



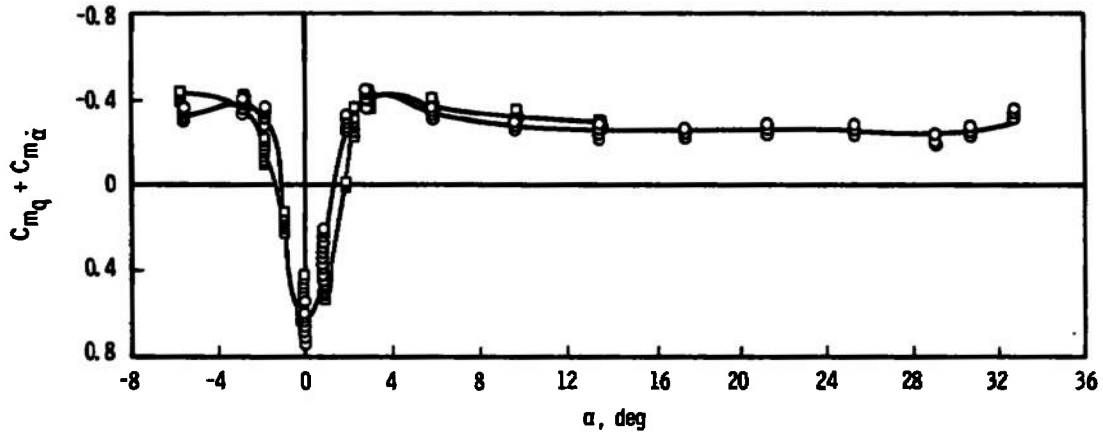
c. $M_\infty = 0.90, Re_d \approx 0.73 \times 10^6$



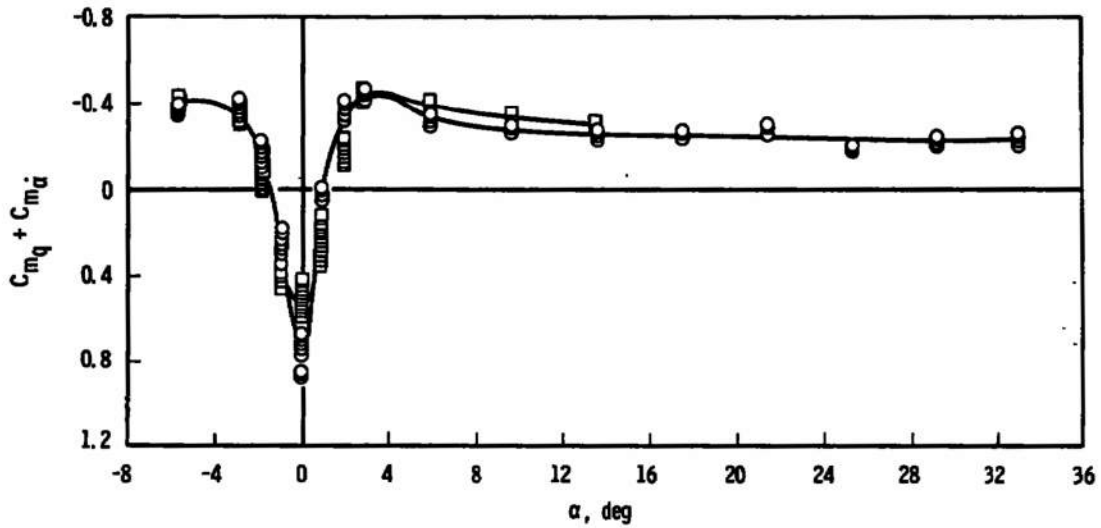
d. $M_\infty = 1.00, Re_d \approx 0.69 \times 10^6$

Fig. 21 Effect of Base Fairing, Config. 721M and 720M, $x_{cg}/l = 1.252$

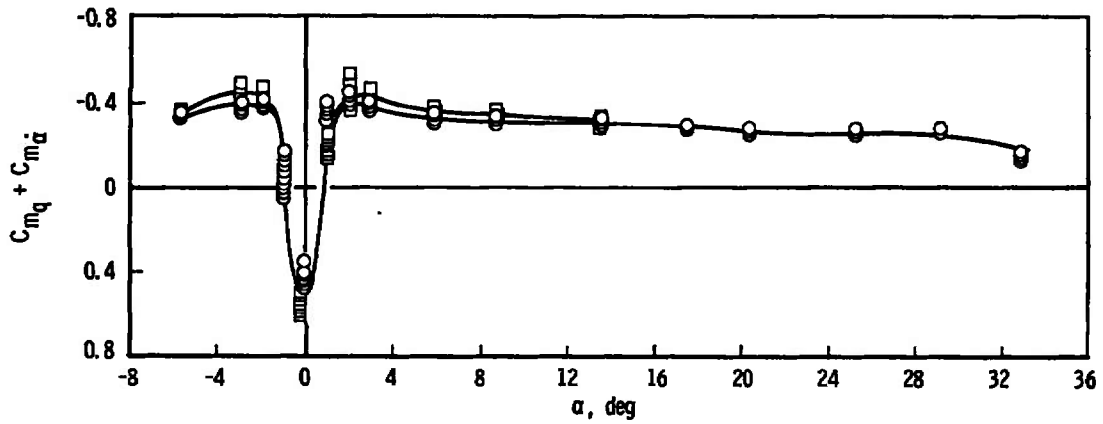
Symbol	Config.
○	721M
□	720M



e. $M_\infty = 1.10, Re_d \approx 0.65 \times 10^6$



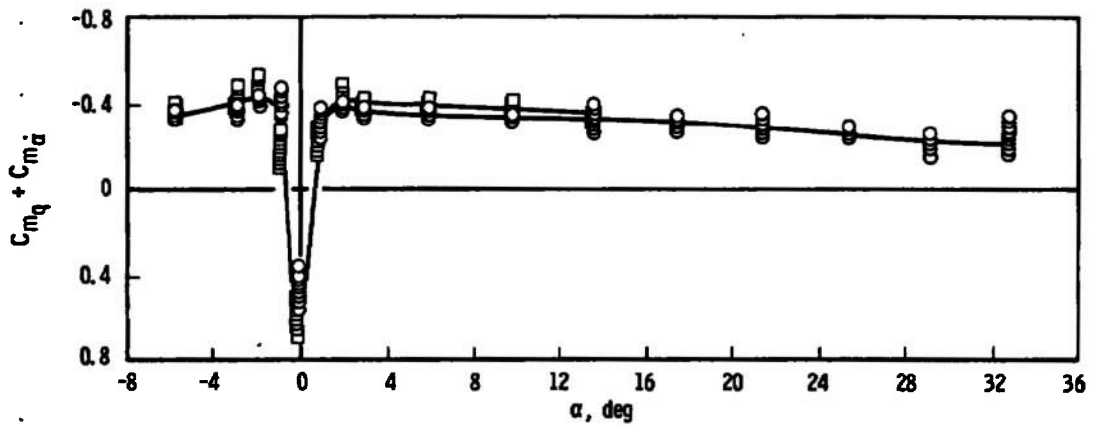
f. $M_\infty = 1.20, Re_d \approx 0.63 \times 10^6$



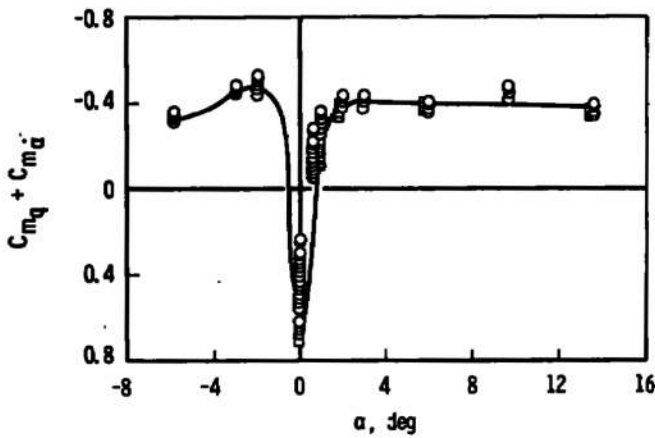
g. $M_\infty = 1.40, Re_d \approx 0.60 \times 10^6$

Fig. 21 Continued

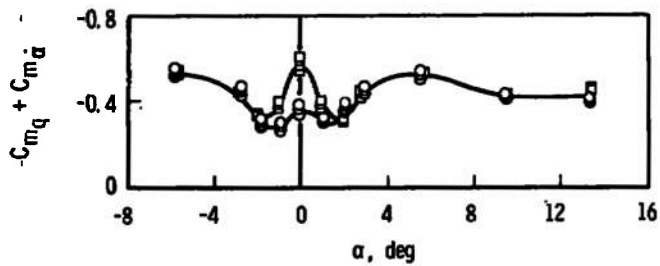
Symbol	Config.
○	721M
□	720M



h. $M_\infty = 1.53, Re_d \approx 0.58 \times 10^6$

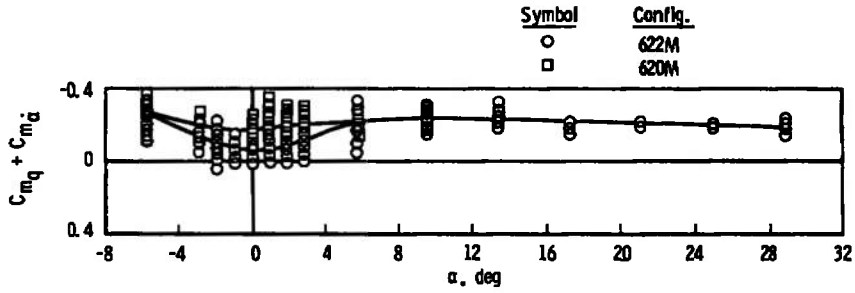


i. $M_\infty = 1.90, Re_d \approx 0.59 \times 10^6$

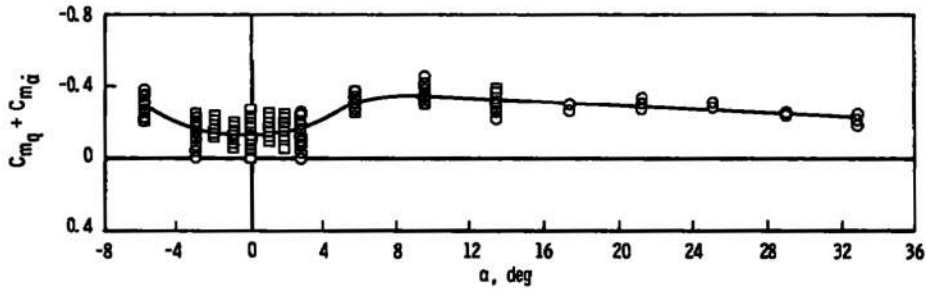


j. $M_\infty = 3.00, Re_d \approx 0.74 \times 10^6$

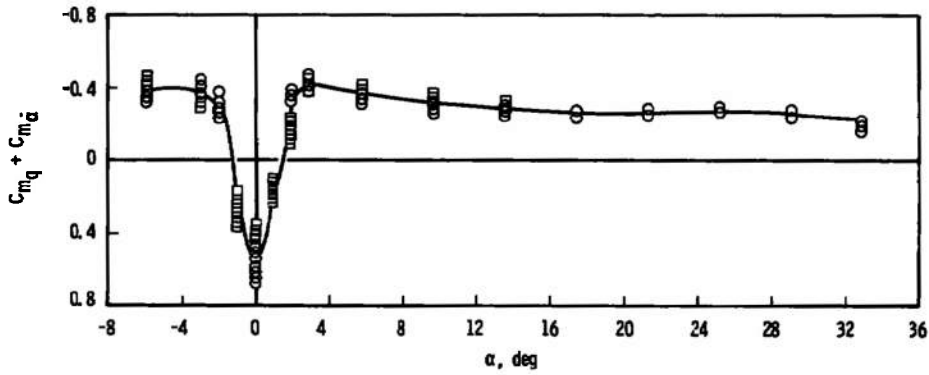
Fig. 21 Concluded



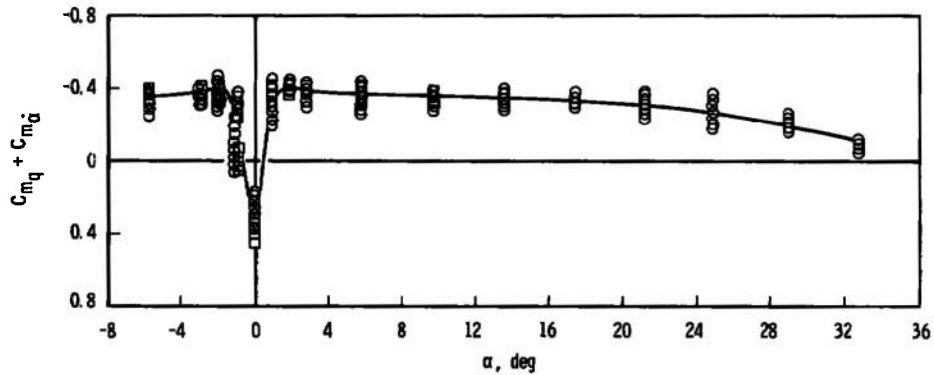
a. $M_\infty = 0.80, Re_d \approx 0.79 \times 10^6$



b. $M_\infty = 1.00, Re_d \approx 0.69 \times 10^6$

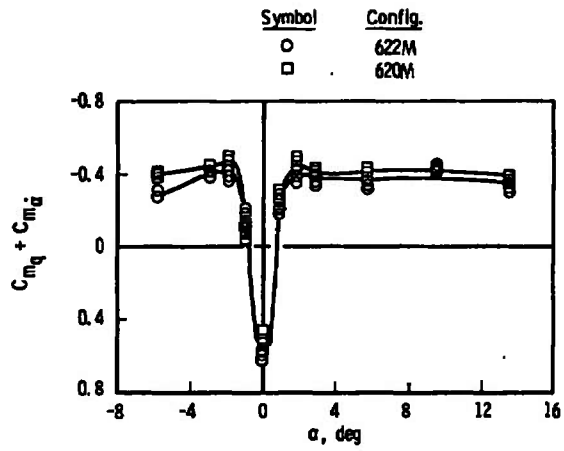


c. $M_\infty = 1.20, Re_d \approx 0.62 \times 10^6$

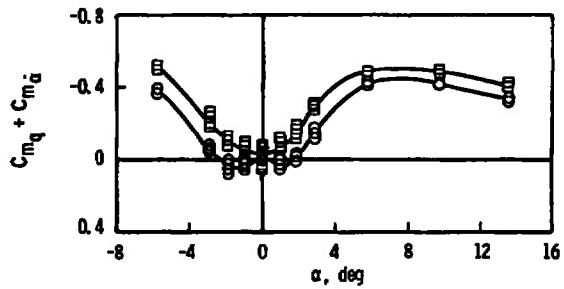


d. $M_\infty = 1.60, Re_d \approx 0.58 \times 10^6$

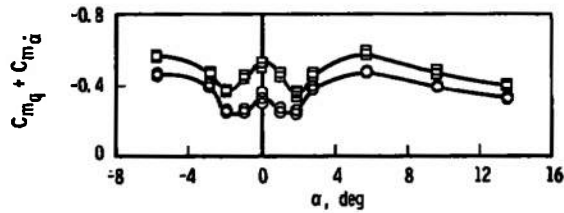
Fig. 22 Effect of Base Fairing, Config. 622M and 620M, $x_{cg}/l = 1.000$



e. $M_\infty = 1.90, Re_d \approx 0.59 \times 10^6$



f. $M_\infty = 2.30, Re_d \approx 0.62 \times 10^6$



g. $M_\infty = 3.00, Re_d \approx 0.75 \times 10^6$

Fig. 22 Concluded

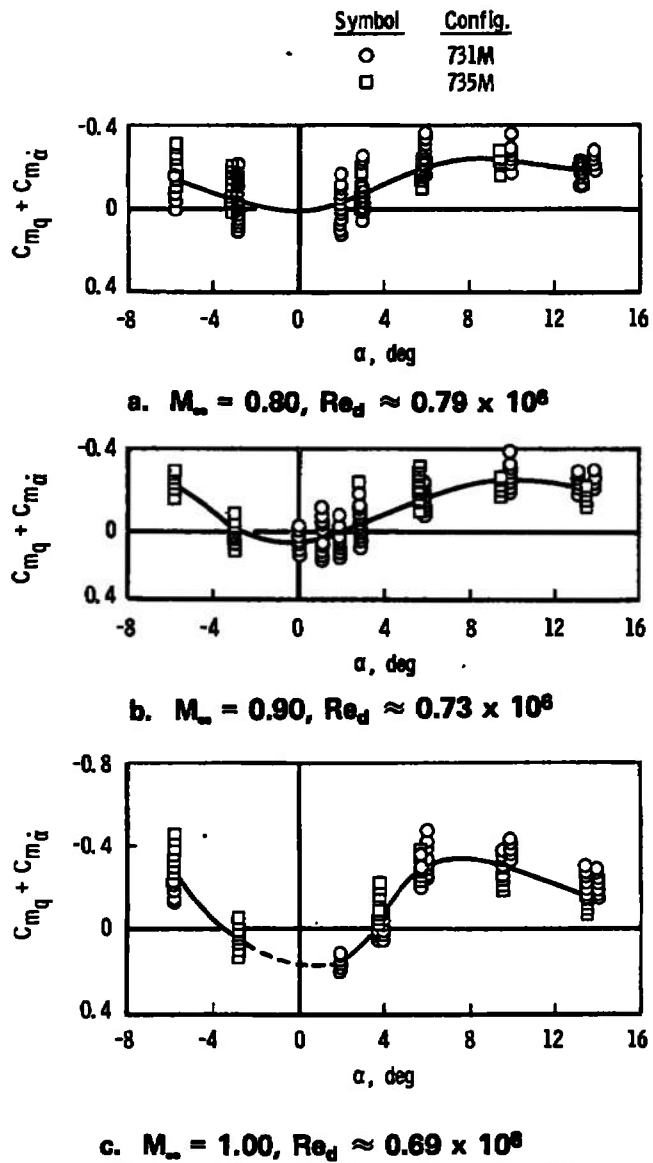
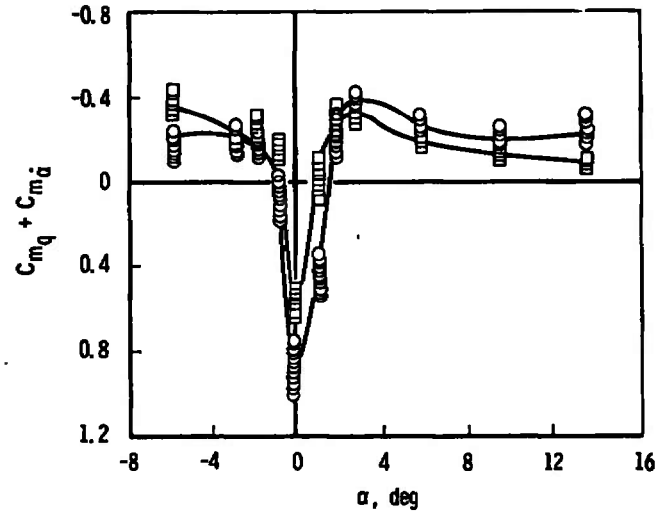
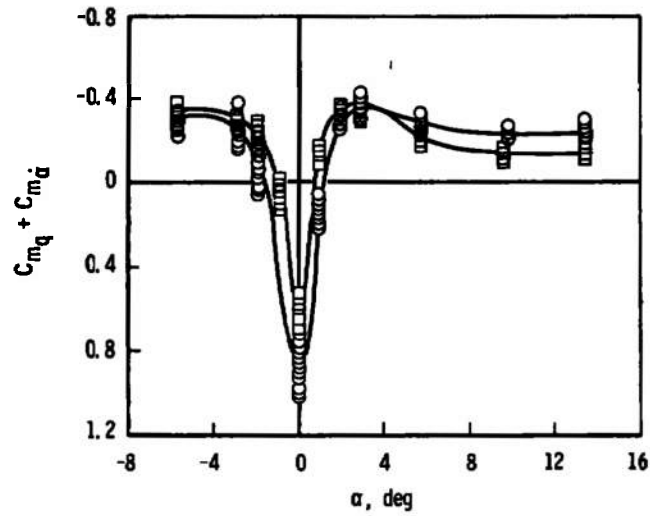


Fig. 23 Effect of Base Fairing, Config. 731M and 735M, $x_{cg}/l = 1.428$

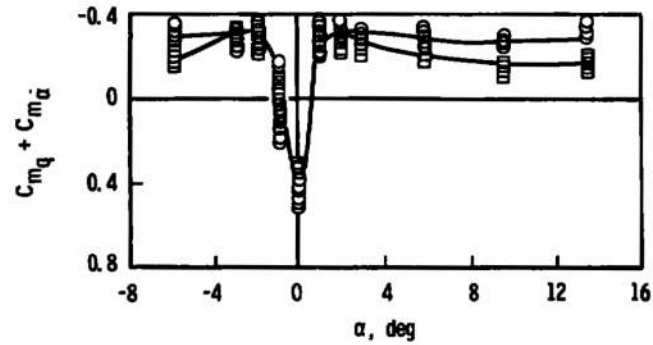
Symbol	Config.
○	731M
□	735M



d. $M_\infty = 1.10, Re_d \approx 0.65 \times 10^6$



e. $M_\infty = 1.20, Re_d \approx 0.62 \times 10^6$



f. $M_\infty = 1.40, Re_d \approx 0.60 \times 10^6$

Fig. 23 Concluded

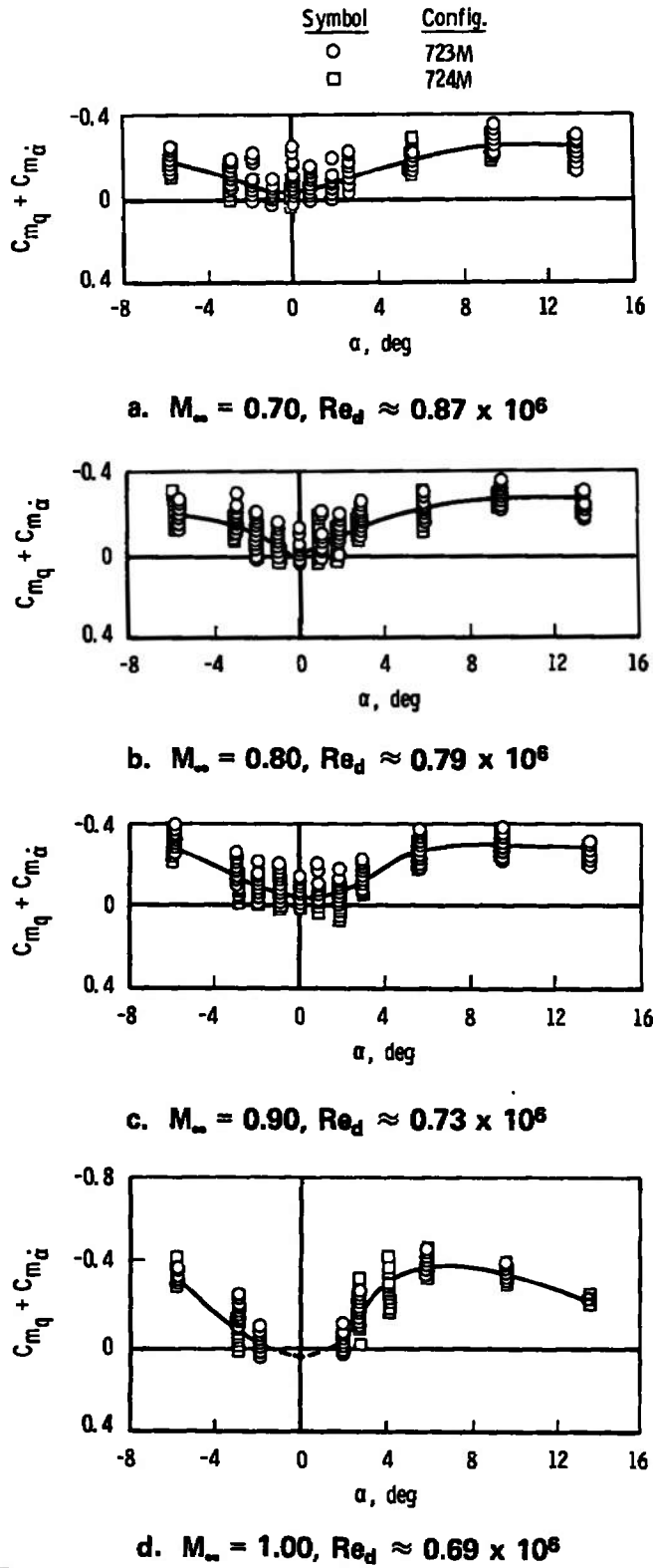
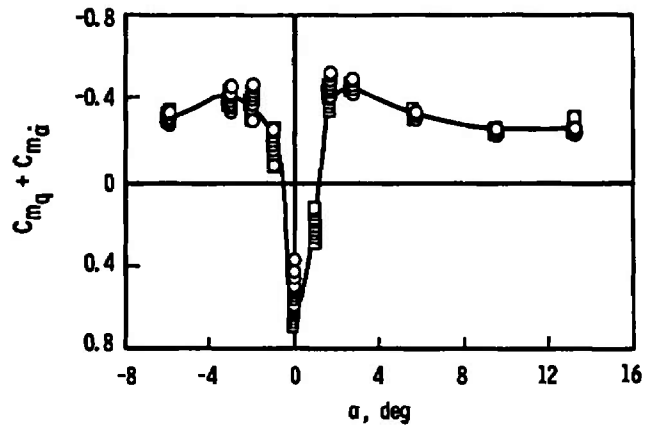
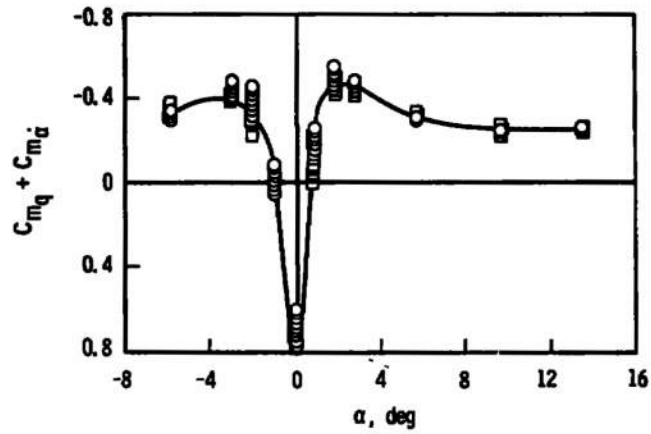


Fig. 24 Effect of Base Fairing, Config. 723M and 724M, $x_{cg}/l = 1.252$

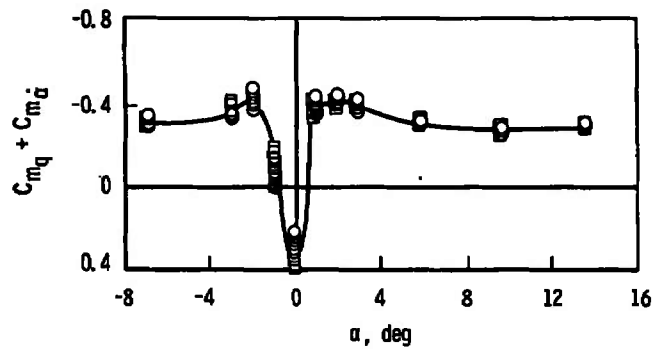
Symbol	Config.
○	723M
□	724M



e. $M_\infty = 1.10, Re_d \approx 0.65 \times 10^6$



f. $M_\infty = 1.20, Re_d \approx 0.62 \times 10^6$



g. $M_\infty = 1.40, Re_d \approx 0.59 \times 10^6$

Fig. 24 Concluded

TABLE I
MODEL CONDITIONS

Config.	Schedule	θ_c , deg	x_{cg}/l	x_{cg}/d	$\omega d/2V_\infty \times 10^2$
620M	B4,† C5, D3,† E7, H2, N1 P2, Q3, R3, S2, U1	60	1.000	0.254	3.80 to 10.26
612M	B4,† C5,† D3,† E7,† E9,* F2,† H2,† K2,† N1,† Q3,† R2,† S2,† T4,† U1,†	60	0.831	0.211	2.94 to 7.95
622M	B4,† B6,* B7,* B8,* C5, C7 D3, D5, E7, E8, F2,† F3,* H2, H3, K2, K3, N1, N2 Q3, S2, U1	60	1.000	0.254	3.04 to 8.34
720M	B4, C5, D3, D6,* E7, F2 H2, K2, M1, Q2, S2,† U1	70	1.252	0.214	3.91 to 10.59
711M	B4,† B5,* C5, C6, D3,† D4,* E7, E8, F2,† F3,* H2, K2 K3, N1, N2, Q3, S2,* U1	70	1.000	0.171	3.05 to 8.31
721M	B4, B5, C5, C6, D3, D4 E7, E8, F2, F3, H2, H3 K2, K3, M2, N1, P1,† Q1 Q3, Q4, R1,† S1, S2,† S3, T1, T2, T5, U1	70	1.252	0.214	2.91 to 7.90
731M	A4,* B4,† B5,* C5, C6,* D3 D4,* E7, E8,* F2, F3,* H2 H3,* K2, K3,* N1,† N2,* Q3,† S2,*	70	1.428	0.244	3.16 to 8.83
723M	B4, C5, D3, E7, F2, H2 K2	70	1.252	0.214	4.61 to 8.31
724M	B4, C5, D3, E7, F2, H2 K2, M1,† N1,† P2, Q3,† R2,† S2,† T3,† U2,*	70	1.252	0.214	3.26 to 8.29
734M*	B3, C4, D2, E6, F1, H1 K1, M1	70	1.428	0.244	4.10 to 7.80
735M	C5, D3, E7, F2, H2, K2 M1,*	70	1.428	0.244	4.02 to 6.81
610N†	B1, E2, J2, L2	60	0.704	0.189	2.96 to 5.53
611N	B1,† B2,* E2,† E5,* J2,† J4,* L2,† L4,*	60	0.704	0.189	2.93 to 5.53
631N*	C2, C3, D1, E3, G1, J1 L1	60	1.000	0.268	2.59 to 4.31
711N	A1, E2, G2, J2, L2	70	1.066	0.178	3.12 to 6.72
741N*	A3, C1, E1, E4, G1, G3 J1, J3, L1, L3	70	1.467	0.245	2.43 to 5.23
742N*	A2, E1, J1, L1	70	1.467	0.245	2.42 to 5.19

*Data not presented

† Selected portions of data presented

$\theta \approx \pm 1.8$ deg

TABLE I (Continued)

<u>Schedule</u>	<u>M_∞</u>	<u>Re_d x 10⁻⁶</u>	<u>α, deg</u>
A1	0.60	0.64	2.8 to 21.5
A2	↓	↓	5.8 to 15.5
A3	↓	↓	8.9 to 39.2
A4	↓	1.00	9.9 to 13.9
B1	0.70	0.57	0 to 21.4
B2	↓	↓	25.4 to 39.3
B3	↓	0.87	-5.7 to 9.4
B4	↓	↓	-5.7 to 13.3
B5	↓	↓	13.3 to 30.7
B6	↓	↓	13.3 to 26.8
B7	↓	1.62	12.8
B8	0.71	0.42	13.7
C1	0.80	0.51	0 to 39.1
C2	↓	↓	5.9 to 15.6
C3	↓	0.76	5.8 to 15.4
C4	↓	0.79	-5.7 to 9.4
C5	↓	↓	-5.7 to 13.4
C6	↓	↓	13.4 to 32.7
C7	↓	↓	13.4 to 28.8
D1	0.90	0.47	2.0 to 15.6
D2	↓	0.73	-5.7 to 9.4
D3	↓	↓	-5.7 to 13.4
D4	↓	↓	13.4 to 32.8
D5	↓	↓	13.4 to 30.6
D6	↓	1.46	5.3 to 9.1
E1	1.00	0.44	0 to 15.5
E2	↓	↓	0 to 21.5
E3	↓	↓	2.9 to 15.6
E4	↓	↓	18.2 to 39.2
E5	↓	↓	25.5 to 39.3
E6	↓	0.68	-5.7 to 9.5
E7	↓	↓	-5.8 to 13.5
E8	↓	↓	13.4 to 32.8
E9	↓	1.37	2.6 to 12.9
F1	1.10	0.65	-5.7 to 9.5
F2	↓	↓	-5.8 to 13.5
F3	↓	↓	13.5 to 32.9
G1	1.15	0.41	0 to 15.6
G2	↓	↓	0 to 21.6
G3	↓	↓	18.2 to 36.9
H1	1.20	0.63	-5.8 to 9.6
H2	↓	↓	-5.8 to 13.5
H3	↓	↓	13.5 to 32.9
J1	1.30	0.39	0 to 15.9
J2	↓	↓	0 to 21.5
J3	↓	↓	18.3 to 39.2
J4	↓	↓	25.6 to 39.4
K1	1.40	0.60	-5.9 to 9.6
K2	↓	↓	-5.9 to 13.6
K3	↓	↓	13.5 to 32.9
L1	1.50	0.58	0 to 15.5
L2	↓	↓	0 to 21.3

TABLE I (Concluded)

<u>Schedule</u>	<u>M_∞</u>	<u>Re_d x 10⁻⁶</u>	<u>α, deg</u>
L3	1.50	0.58	18.1 to 36.6
L4	↓	↓	25.3 to 33.1
M1	1.53	↓	-5.8 to 13.6
M2	↓	↓	-5.9 to 32.6
N1	1.60	↓	-5.8 to 13.6
N2	↓	↓	13.5 to 32.9
P1	1.75	0.60	0 to 0.9
P2	↓	↓	0
Q1	1.90	0.37	0 to 5.8
Q2	↓	0.59	0 to 13.6
Q3	↓	↓	-5.8 to 13.6
Q4	↓	1.02	0 to 5.6
R1	2.10	0.60	0 to 0.9
R2	↓	↓	-5.7 to 13.5
R3	↓	↓	0
S1	2.30	0.39	0 to 5.9
S2	↓	0.62	-5.8 to 13.6
S3	↓	1.11	-5.6 to 5.7
T1	2.65	0.43	0 to 5.8
T2	↓	0.69	0 to 5.8
T3	↓	↓	-2.9 to 13.6
T4	↓	↓	-5.8 to 13.5
T5	↓	1.12	0.9 to 5.5
U1	3.00	0.75	-5.8 to 13.5
U2	↓	↓	-4.94

TABLE II
TUNNEL CONDITIONS

M_∞	$Re_d \times 10^{-6}$ Config. ABCM	$Re_d \times 10^{-6}$ Config. ABCN	p_{O_2} psia	T_{O_2} °R	q_∞ psia	V_∞ ft/sec
0.60	1.00	0.64	3.52	571	0.69	678
0.70	0.87	0.57	2.80	574	0.69	786
0.70	1.62		5.19	575	1.28	786
0.71	0.42		1.31	570	0.33	794
0.80	0.79	0.51	2.36	574	0.69	885
0.80		0.76	3.54	575	1.04	886
0.90	0.73	0.47	2.07	575	0.69	982
0.90	1.46		4.13	575	1.38	982
1.00	0.68	0.44	1.87	585	0.69	1073
1.00	1.37		3.75	574	1.38	1073
1.10	0.65		1.75	575	0.69	1161
1.15		0.41	1.71	575	0.70	1202
1.20	0.63		1.69	574	0.70	1243
1.30		0.39	1.64	577	0.70	1323
1.40	0.60		1.62	576	0.70	1396
1.50		0.58	2.49	576	1.07	1466
1.53	0.58		1.62	575	0.69	1485
1.60	0.58		1.66	579	0.70	1535
1.75	0.60		1.72	561	0.69	1598
1.90	0.37		1.11	558	0.42	1679
1.90	0.59		1.85	573	0.70	1700
1.90	1.02		3.22	576	1.21	1703
2.10	0.60		2.06	571	0.69	1794
2.30	0.39		1.41	554	0.42	1849
2.30	0.62		2.36	577	0.70	1890
2.30	1.11		4.14	568	1.22	1874
2.65	0.43		1.84	554	0.42	1971
2.65	0.69		3.05	566	0.69	1993
2.65	1.12		5.33	595	1.21	2044
3.00	0.75		4.05	571	0.69	2100

DOCUMENT CONTROL DATA - R & D

(Security classification of title, body of abstract and indexing annotation must be entered when the overall report is classified)

1. ORIGINATING ACTIVITY (Corporate author) Arnold Engineering Development Center ARO, Inc., Operating Contractor Arnold Air Force Station, Tennessee 37389		2a. REPORT SECURITY CLASSIFICATION UNCLASSIFIED	
		2b. GROUP N/A	
3. REPORT TITLE DAMPING-IN-PITCH DERIVATIVES OF 120- AND 140-DEG BLUNTED CONES AT MACH NUMBERS FROM 0.6 THROUGH 3			
4. DESCRIPTIVE NOTES (Type of report and inclusive dates) Final Report September 3 to November 1, 1969			
5. AUTHOR(S) (First name, middle initial, last name) B. L. Uselton, T. O. Shadow, and A. C. Mansfield, ARO, Inc.			
6. REPORT DATE April 1970		7a. TOTAL NO. OF PAGES 63	7b. NO. OF REFS 17
8a. CONTRACT OR GRANT NO. F40600-69-C-0001		9a. ORIGINATOR'S REPORT NUMBER(S) AEDC-TR-70-49	
b. Program Element 921E 5			
c.		9b. OTHER REPORT NO(S) (Any other numbers that may be assigned)	
d.		This document has been approved for public release and sale. Its distribution is unlimited.	
10. DISTRIBUTION STATEMENT Each transmittal of this document outside the agencies of the U. S. Government must have prior approval of NASA, Langley Research Center, Hampton, Virginia 23365.			
11. SUPPLEMENTARY NOTES Available in DDC.		12. SPONSORING MILITARY ACTIVITY NASA, Langley Research Center, Hampton, Virginia 23365	
13. ABSTRACT Wind tunnel tests were conducted to determine the damping-in-pitch derivatives ($C_{m\dot{\alpha}} + C_{m\dot{\alpha}}$) of 120- and 140-deg blunted, conical models with and without base fairings. Measurements were made with a forced-oscillation dynamic balance as the model oscillated ± 1.8 deg at angles of attack ranging from -5.9 to 39.4 deg. Data were obtained at nominal Mach numbers of 0.6 to 3 and at free-stream Reynolds numbers, based on maximum model diameter, ranging from 0.37×10^6 to 1.62×10^6 . In general for all configurations the damping derivatives at $\alpha = 0$ were a strong nonlinear function of Mach number and showed the models to be dynamically unstable at Mach numbers from about 1.1 to 2.1. However, as angle of attack increased, model stability increased and the derivatives were found to vary in a less nonlinear manner with Mach number. At $M_\infty = 1.9, 2.3,$ and 2.65 Reynolds number effects were investigated and it was noted that the damping-in-pitch derivatives were influenced strongly by Reynolds number. Addition of different base fairings produced no large changes in the damping derivatives. Each transmittal of this document outside the agencies of the U. S. Government must have prior approval of NASA, Langley Research Center, Hampton, Virginia 23365.			

14.

KEY WORDS

LINK A

LINK B

LINK C

ROLE

WT

ROLE

WT

ROLE

WT

conical bodies

pitching

transonic wind tunnels

supersonic wind tunnels

longitudinal stability

- 1. Blunt cones
- 2. Cones - - Stability
- 3 . 1. - - Damping in pitch

1 - 2